

T-4807

**NUMERICAL DETERMINATION OF
SCATTERED FIELD AMPLITUDES FOR
ROUGH SURFACES**

**ARTHUR LAKES LIBRARY
COLORADO SCHOOL OF MINES
GOLDEN, CO 80401**

by
RICHARD C. McNAMARA

ProQuest Number: 10794158

All rights reserved

INFORMATION TO ALL USERS

The quality of this reproduction is dependent upon the quality of the copy submitted.

In the unlikely event that the author did not send a complete manuscript and there are missing pages, these will be noted. Also, if material had to be removed, a note will indicate the deletion.



ProQuest 10794158

Published by ProQuest LLC (2018). Copyright of the Dissertation is held by the Author.

All rights reserved.

This work is protected against unauthorized copying under Title 17, United States Code
Microform Edition © ProQuest LLC.

ProQuest LLC.
789 East Eisenhower Parkway
P.O. Box 1346
Ann Arbor, MI 48106 – 1346

A thesis submitted to the Faculty and the Board of Trustees of the Colorado School of Mines in partial fulfillment of the requirements for the degree of Master of Science (Mathematical and Computer Sciences).

Golden, Colorado

Date 6/16/95

Signed: Richard C. McNamara
RICHARD C. McNAMARA

Approved: John A. DeSanto
Dr. John A. DeSanto
Professor of Mathematical and
Computer Sciences
Thesis Advisor

Golden, Colorado

Date 6/19/95

Graeme Fairweather
Dr. Graeme Fairweather
Professor and Head,
Department of Mathematical and
Computer Sciences

ABSTRACT

In theory, when a plane wave strikes a perfectly-reflecting surface, the resulting scattered field is comprised of a continuous spectrum of waves. Upon applying Dirichlet boundary conditions to the surface, one can construct what is referred to as a Spectral-Coordinate formalism for the scattered amplitudes, which takes the form of an integral equation of the first kind on an infinite interval. If the surface is assumed to be periodic, the spectrum of scattered amplitudes is discrete, and the integration is over a single period.

The problem will be approached numerically, using a pseudo-inverse SVD technique, and the performance of the resulting code will be evaluated via a complete analysis of the classical sinusoidal surface problem. A particularly interesting feature of the code is the high level of accuracy attained for near-grazing incident fields.

Although the sinusoidal surface receives most of the attention in this paper, the code can be applied to arbitrary surface geometries. Thus, this work is applicable to a wide variety of actual physical problems.

TABLE OF CONTENTS

ABSTRACT	iii
LIST OF TABLES	v
LIST OF FIGURES	vi
ACKNOWLEDGEMENTS	vii
1 INTRODUCTION	1
2 INTEGRAL EQUATIONS FOR ARBITRARY SURFACES	7
3 INTEGRAL EQUATIONS FOR PERIODIC SURFACES	21
4 DISCRETIZATION OF THE INTEGRAL EQUATION	29
5 DRIVER FOR NUMERICAL SOLUTION	38
6 NUMERICAL RESULTS	51
7 CONCLUSIONS	71
REFERENCES	76
APPENDIX A - DRIVER CODE	78

LIST OF TABLES

6.1	Bragg Indices and Scattered Angles, $L \sim 20\lambda_1$	62
6.2	Results for $L = 15.9\lambda_1$, $(\frac{d}{L}) = 0.100$, and $\theta_{inc} = 0^\circ$	68
6.3	Results for $L = 15.9\lambda_1$, $(\frac{d}{L}) = 0.195$, and $\theta_{inc} = 0^\circ$	69
6.4	Results for $L = 15.9\lambda_1$, $(\frac{d}{L}) = 0.100$, and $\theta_{inc} = 89.5^\circ$	70

LIST OF FIGURES

1.1	Geometry of the Problem	1
1.2	Incident and Scattered Plane Waves	4
2.1	Closed Contour C_{123451}	8
5.1	Location of Spectral Samples	40
5.2	Staggered Sampling for x	45
6.1	Sinusoidal Surface	51
6.2	Error vs n , $L \sim 20\lambda_1$, $\theta_{inc} = 0^\circ$	57
6.3	Error vs $(\frac{d}{L})$, where $L \sim 20\lambda_1$, for selected values of θ_{inc}	61
6.4	Error vs θ_{inc} , where $L \sim 20\lambda_1$, for selected values of $(\frac{d}{L})$	63
6.5	Error vs $(\frac{d}{L})$, where $\theta_{inc} = 0^\circ$, for $L = 3, 10, \text{ and } 20$	64

ACKNOWLEDGEMENTS

I would like to thank the members of my committee, Dr. John A. DeSanto, Dr. Steven A. Pruess, and Dr. Erik S. Van Vleck, for enthusiastically sharing their knowledge and experience in assisting me with this endeavor. Not only did they offer advice regarding the applications of standard techniques, but they also encouraged me to exercise creativity. In addition, I extend special thanks to Dr. DeSanto for his patient guidance throughout the project, and for providing me with the opportunity to learn a great deal about his field of special interest. I would also like to express appreciation to my friend and colleague, Charles Farris, for his hard work in preparing the typed version of this manuscript.

Finally, I will take this opportunity to acknowledge the continuous encouragement I received from my family throughout the pursuit of my Master's Degree. Their support has been highly instrumental in enabling me to meet the challenges involved in graduate-level study.

Chapter 1

INTRODUCTION

Consider a perfectly-reflecting arbitrary surface of infinite length, as depicted in Figure (1.1). The geometry of the surface is described by the function $z = s(x)$, and the value $z = H$ is the highest excursion of the surface in the z -direction. The region denoted by V_1 is defined by $s(x) < z < H$, and the region denoted by A is the region above the highest surface excursion, defined by $z > H$.

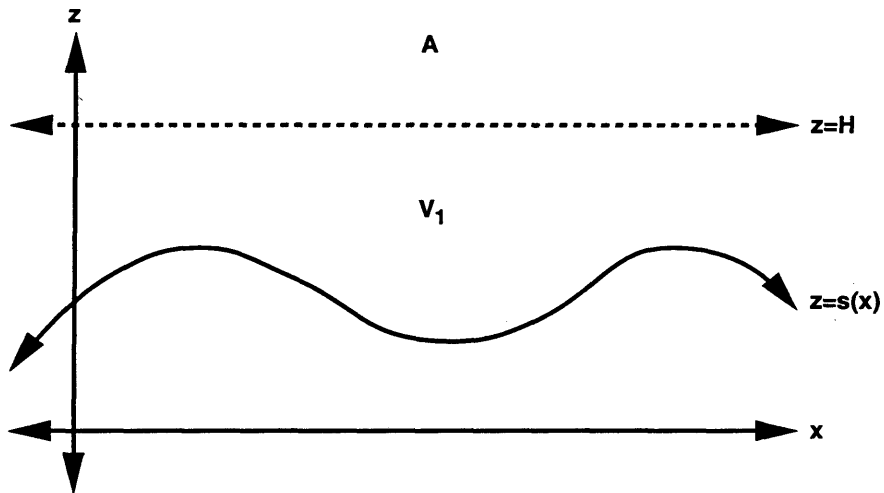


FIG. 1.1. Geometry of the Problem

Consider also the presence of a single source, located somewhere in region A , which generates an incident field, $\psi^0(x, z)$. When the surface is subjected to ψ^0 , a scattered field, $\psi^{sc}(x, z)$, is produced. The resulting total field can be expressed as

the sum of the incident field and the scattered field so that

$$\psi(x, z) = \psi^0(x, z) + \psi^{sc}(x, z) \quad (1.1)$$

In acoustics, ψ represents the velocity potential, and in electromagnetics, ψ represents the y -component of the electric field for transverse electric (TE) polarization, or the y -component of the magnetic field for transverse magnetic (TM) polarization.

This thesis deals with the case where the incident field consists of a single plane wave, although much of the theory applies to other types of sources. Even though a true plane wave is of infinite extent, and is therefore impossible to generate, the equations and results developed here are applicable to close facsimiles thereof, which do arise in practice.

Assuming plane-wave incidence, the behavior of the total field is governed by the scalar Helmholtz equation

$$(\partial_l \partial_l + k_1^2) \psi = 0 \quad l = 1, 3 \quad (1.2)$$

Throughout this thesis, tensor differential operators will be utilized so that ∂_l is the gradient operator and $\partial_l \partial_l$ is the two-dimensional Laplacian operator. Thus,

$$\partial_l = \left(\delta_{l1} \frac{\partial}{\partial x} + \delta_{l3} \frac{\partial}{\partial z} \right) = \begin{cases} \frac{\partial}{\partial x} & l = 1 \\ \frac{\partial}{\partial z} & l = 3 \end{cases} \quad (1.3)$$

and

$$\partial_l \partial_l = \partial_1 \partial_1 + \partial_3 \partial_3 = \left(\frac{\partial^2}{\partial x^2} + \frac{\partial^2}{\partial z^2} \right) \quad (1.4)$$

δ_{mn} is the Kronecker delta term, given by

$$\delta_{mn} = \begin{cases} 1 & m = n \\ 0 & m \neq n \end{cases} \quad (1.5)$$

In addition, k_1 is the wave number, and it is related to the wavelength λ_1 of the field by

$$k_1 = \frac{2\pi}{\lambda_1} \quad (1.6)$$

The constants k_1 and λ_1 are associated with regions V_1 and A .

Both ψ^0 and ψ^{sc} must satisfy the Helmholtz equation. Hence,

$$(\partial_l \partial_l + k_1^2) \psi^0 = 0 \quad (1.7)$$

and

$$(\partial_l \partial_l + k_1^2) \psi^{sc} = 0 \quad (1.8)$$

An incident plane wave has an associated incident angle and a scattered plane wave has an associated scattered angle, which we shall denote as θ_{inc} and θ_{sc} , respectively. As a convention, θ_{inc} will represent the angle of the incident ray with respect to the z -axis, and this angle will be considered as positive if the slope of the incident ray, $\frac{dz}{dx}$, is negative, and it will be considered as negative if $\frac{dz}{dx}$ is positive. Similarly, θ_{sc} represents the angle of the scattered ray with respect to the z -axis; however, it will be taken as positive if the slope of the scattered ray, $\frac{dz}{dx}$, is positive, and it will be taken as negative if $\frac{dz}{dx}$ is negative. Thus, for plane waves oriented as in Figure (1.2), both θ_{inc} and θ_{sc} are positive.

A spectral representation of an incident plane wave in a homogeneous medium

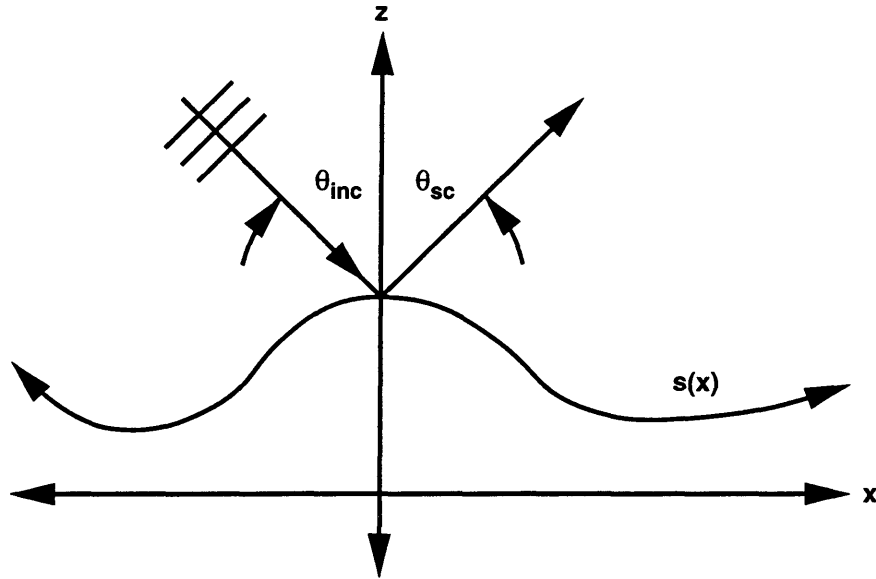


FIG. 1.2. Incident and Scattered Plane Waves

can be given as

$$\psi^0(x, z) = D e^{ik_1(\alpha x - \beta z)} \quad (1.9)$$

where D is the amplitude, $\alpha = \sin(\theta_{inc})$, and $\beta = \cos(\theta_{inc})$. This representation of $\psi^0(x, z)$ is indeed a solution of Equation (1.7). A spectral representation of a continuous set of scattered plane waves in a homogeneous medium can be given by

$$\psi^{sc}(x, z) = \int_{-\infty}^{\infty} A(\mu) e^{ik_1(\mu x + mz)} d\mu \quad (1.10)$$

where m is defined as

$$m = \begin{cases} +\sqrt{1 - \mu^2} & |\mu| \leq 1 \\ +i\sqrt{\mu^2 - 1} & 1 \leq |\mu| \end{cases} \quad (1.11)$$

and the function $A(\mu)$ represents the scattered amplitudes. Both upgoing scattered waves and nonradiating surface waves are accounted for in the representation given by Equation (1.10).

Since region A is assumed to be homogeneous in nature, Equations (1.9) - (1.11) are valid in that region. On the other hand, region V_1 is inhomogeneous due to the presence of the surface. Thus, Equations (1.9) - (1.11) are in general invalid in region V_1 , although they are approximately correct for certain geometries. The results of the work in this thesis will only be applied to region A .

It should be noted that we have narrowed the scope of the problem to a time-independent scenario. The time-dependent field Ψ must satisfy the wave equation

$$\left(\partial_l \partial_l - \left(\frac{1}{c^2} \right) \frac{\partial^2}{\partial t^2} \right) \Psi = 0 \quad (1.12)$$

where c is the wave speed. The solution of Equation (1.12) involves separation of variables, and we assume that

$$\Psi(x, z, t) = \psi(x, z) e^{-i\omega t} \quad (1.13)$$

where the angular frequency ω satisfies $k_1 = \frac{\omega}{c}$. In this thesis, we will only be concerned with the spatial component of the separation of variables, given by Equation (1.2).

Combining Equations (1.1) and (1.10) gives

$$\psi(x, z) = \psi^0(x, z) + \int_{-\infty}^{\infty} A(\mu) e^{ik_1(\mu x + mz)} d\mu \quad (1.14)$$

and since we are assuming plane-wave incidence, ψ^0 is given by Equation (1.9). The

preceding development of Equation (1.14) was based on the work of DeSanto [1].

The exponential kernel in Equation (1.14) is in “Spectral-Coordinate” (SC) form, where the scattered field is expressed as a set of spectral waves. Each element of the spectrum has an associated scattered amplitude $A(\mu)$, which at this stage of the thesis is the only unknown term on the right-hand side of Equation (1.14). In addition, although the spectrum is continuous for an arbitrary surface, as is implied in Equation (1.14), we shall soon see that a periodic surface elicits a discrete spectrum.

The purpose of this thesis is to demonstrate the derivation of the integral equations for $A(\mu)$ associated with periodic surfaces and soft (i.e. Dirichlet) boundary conditions, and then to explore numerical techniques for obtaining the desired scattered amplitudes from those equations. Once the scattered amplitudes have been determined, Equation (1.14) can be used to provide a complete description of the total field in region A .

Chapter 2

INTEGRAL EQUATIONS FOR ARBITRARY SURFACES

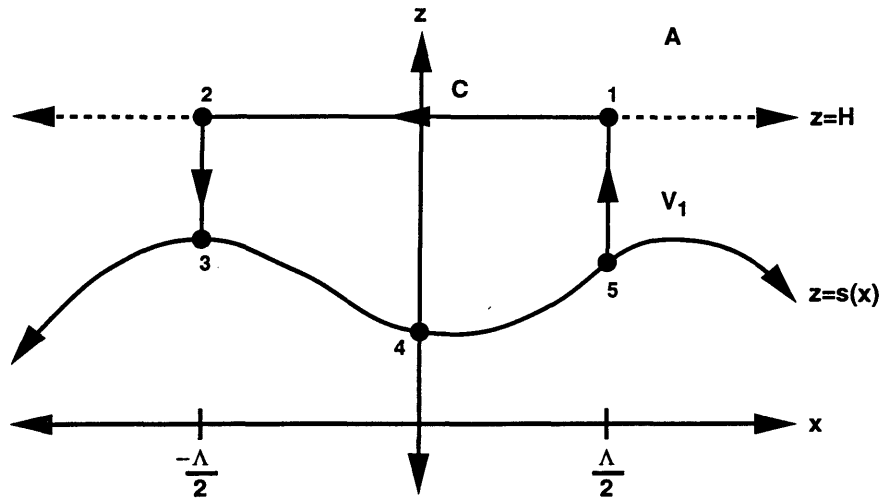
This chapter provides a derivation of the integral equations for the scattered amplitudes $A(\mu)$ associated with an incident plane wave, a perfectly-reflecting arbitrary surface, and Dirichlet boundary conditions. This derivation follows the approach outlined in DeSanto's paper [1], and it is included here in order to provide motivation for the resulting equations. Many steps which have been omitted in DeSanto's work have been included here in order to provide additional insight for those readers who are unfamiliar with the Spectral-Coordinate formalism.

Consider the construction of a closed contour $C = C_{123451}$, as shown in Figure (2.1). Nodes 1 and 2 lie on the line $z = H$, and nodes 3, 4, and 5 lie on the surface $z = s(x)$. The entire interior of the contour lies in the region V_1 introduced in Figure (1.1). The contour is temporarily closed by the inclusion of segments $\overline{23}$ and $\overline{51}$ at $x = \pm \frac{\Lambda}{2}$, but since we assume that the surface is of infinite extent, we shall eventually let Λ approach infinity, so as to enclose all of V_1 .

Auxiliary functions G^\pm , which are plane-wave states for waves travelling in the $\pm z$ -direction, are introduced as

$$G^\pm(x, z) = e^{ik_1(\pm\gamma z - \zeta x)} \quad (2.1)$$

where the parameters γ and ζ are analogous to the parameters m and μ , respectively,

FIG. 2.1. Closed Contour C_{123451}

in Equations (1.10), (1.11), and (1.14). Notice that G^\pm satisfies

$$(\partial_l \partial_l + k_1^2) G^\pm = 0 \quad l = 1, 3 \quad (2.2)$$

We can use Equations (1.2) and (2.2) to establish

$$\psi_1 (\partial_l \partial_l + k_1^2) G^\pm - G^\pm (\partial_l \partial_l + k_1^2) \psi_1 = 0 \quad (2.3)$$

from which it follows that

$$\psi_1 \partial_l \partial_l G^\pm - G^\pm \partial_l \partial_l \psi_1 = 0 \quad (2.4)$$

The notation $\psi = \psi_1$ has been adopted since the region inside contour C lies in V_1 .

Next, one can apply the vector identity

$$\Phi \partial_l v = \partial_l(\Phi v) - v(\partial_l \Phi) \quad (2.5)$$

to both terms in Equation (2.4). In Equation (2.5), Φ is an arbitrary scalar function and v is an arbitrary vector-valued function. Letting $\Phi \equiv \psi_1$ and $v \equiv \partial_l G^\pm$, we obtain

$$\partial_l(\psi_1 \partial_l G^\pm - G^\pm \partial_l \psi_1) = 0 \quad (2.6)$$

Next, we construct the characteristic function

$$\Theta(x, z) = \Theta(z - s(x))\Theta(H - z)\Theta\left(x + \frac{\Lambda}{2}\right)\Theta\left(\frac{\Lambda}{2} - x\right) \quad (2.7)$$

where $\Theta(t)$ is the Heaviside step function. The characteristic function defines the region enclosed by C in the way that for any point (x_0, z_0) ,

$$\Theta(x_0, z_0) = \begin{cases} 1 & (x_0, z_0) \text{ is inside } C \\ 0 & (x_0, z_0) \text{ is outside } C \end{cases} \quad (2.8)$$

In order to simplify the notation involved in the upcoming steps, we let

$$u_l(x, z) = (\psi_1 \partial_l G^\pm - G^\pm \partial_l \psi_1) \quad l = 1, 3 \quad (2.9)$$

Thus,

$$\partial_l u_l = \partial_1 u_1 + \partial_3 u_3 \quad (2.10)$$

where

$$\partial_1 u_1 = \partial_1(\psi_1 \partial_1 G^\pm - G^\pm \partial_1 \psi_1)$$

$$\partial_3 u_3 = \partial_3(\psi_1 \partial_3 G^\pm - G^\pm \partial_3 \psi_1) \quad (2.11)$$

So, we multiply both sides of Equation (2.6) by $\Theta(x, z)$, then integrate both sides over the entire $x - z$ plane, giving

$$\int_{-\infty}^{\infty} \int_{-\infty}^{\infty} \partial_1 u_1(x, z) \Theta(x, z) dx dz + \int_{-\infty}^{\infty} \int_{-\infty}^{\infty} \partial_3 u_3(x, z) \Theta(x, z) dx dz = 0 \quad (2.12)$$

We integrate both terms by parts to obtain

$$\begin{aligned} & \int_{-\infty}^{\infty} [u_1 \Theta(x, z)|_{-\infty}^{\infty}] dz + \int_{-\infty}^{\infty} \int_{-\infty}^{\infty} u_1 \partial_1 \Theta(x, z) dx dz \\ & + \int_{-\infty}^{\infty} [u_3 \Theta(x, z)|_{-\infty}^{\infty}] dx + \int_{-\infty}^{\infty} \int_{-\infty}^{\infty} u_3 \partial_3 \Theta(x, z) dx dz = 0 \end{aligned} \quad (2.13)$$

From Equation (2.7), it is clear that $\lim_{z \rightarrow \pm\infty} \Theta(x, z) = 0$, so that the second partially-integrated term in Equation (2.13) is zero. We can rewrite Equation (2.13) with the remaining three terms as

$$\int_{-\infty}^{\infty} \lim_{\Lambda \rightarrow \infty} \left[(u_1(x, z) \Theta(x, z)|_{-\frac{\Lambda}{2}}^{\frac{\Lambda}{2}}) + \int_{-\frac{\Lambda}{2}}^{\frac{\Lambda}{2}} u_1(x, z) \partial_1 \Theta(x, z) dx \right] dz = 0 \quad (2.14)$$

We take the gradient of $\Theta(x, z)$, while recalling that the derivative of the Heaviside step function is the Dirac delta function. Hence,

$$\begin{aligned} \partial_l \Theta(x, z) &= [\delta_{l3} - \delta_{l1} s'(x)] \delta(z - s(x)) \Theta(H - z) \Theta(x + \frac{\Lambda}{2}) \Theta(\frac{\Lambda}{2} - x) \\ &+ \delta_{l1} \Theta(z - s(x)) \Theta(H - z) \delta(x + \frac{\Lambda}{2}) \Theta(\frac{\Lambda}{2} - x) \\ &- \delta_{l1} \Theta(z - s(x)) \Theta(H - z) \Theta(x + \frac{\Lambda}{2}) \delta(\frac{\Lambda}{2} - x) \\ &- \delta_{l3} \Theta(z - s(x)) \delta(H - z) \Theta(x + \frac{\Lambda}{2}) \Theta(\frac{\Lambda}{2} - x) \end{aligned} \quad (2.15)$$

The term $(\delta_{l3} - \delta_{l1}s'(x))$ is a vector normal to the surface and we shall denote it as

$$n_l(x) = (\delta_{l3} - \delta_{l1}s'(x)) \quad (2.16)$$

So, we consider the following integral, which appears in Equation (2.14), and use Equations (2.15) and (2.16) to obtain

$$\begin{aligned} & \int_{-\frac{\Lambda}{2}}^{\frac{\Lambda}{2}} u_l(x, z) \partial_l \Theta(x, z) dx \\ &= \int_{-\frac{\Lambda}{2}}^{\frac{\Lambda}{2}} u_l(x, z) \delta(z - s(x)) \Theta(H - z) \Theta\left(x + \frac{\Lambda}{2}\right) \Theta\left(\frac{\Lambda}{2} - x\right) n_l(x) dx \\ &+ \delta_{l1} \Theta(H - z) \Theta(\Lambda) [\Theta(z - s(-\frac{\Lambda}{2})) u_l(-\frac{\Lambda}{2}, z) - \Theta(z - s(\frac{\Lambda}{2})) u_l(\frac{\Lambda}{2}, z)] \\ &- \delta_{l3} \int_{-\frac{\Lambda}{2}}^{\frac{\Lambda}{2}} u_l(x, z) \Theta(z - s(x)) \delta(H - z) \Theta\left(x + \frac{\Lambda}{2}\right) \Theta\left(\frac{\Lambda}{2} - x\right) dx \end{aligned} \quad (2.17)$$

Note that the other term in the integrand of Equation (2.14) is

$$u_1(x, z) \Theta(x, z) \Big|_{-\frac{\Lambda}{2}}^{\frac{\Lambda}{2}} = \Theta\left(\frac{\Lambda}{2}, z\right) u_1\left(\frac{\Lambda}{2}, z\right) - \Theta\left(-\frac{\Lambda}{2}, z\right) u_1\left(-\frac{\Lambda}{2}, z\right) \quad (2.18)$$

Thus, the middle term of Equation (2.17) plus the term from Equation (2.18) sum to a term on the order of u_1 . The remaining two terms in Equation (2.17) are integrals of u_l times scalar terms and $n_l(x)$, the result of which is on the order of Λu_l . Hence, as Λ approaches infinity, the former two are dominated asymptotically by the latter two, which is equivalent to saying that the contributions of the two vertical integrals in contour C in Figure (2.1) are negligible (asymptotically of higher order) in DeSanto's Green's Theorem approach [2]. Therefore, letting Λ approach infinity and substituting the two dominant terms from Equation (2.17) into Equation (2.14), and changing the

order of integration gives

$$\begin{aligned} & \int_{-\infty}^{\infty} [\psi_1(x, H) \partial_3 G^\pm(x, H) - G^\pm(x, H) \partial_3 \psi_1(x, H)] dx \\ &= \int_{-\infty}^{\infty} [\psi_1(x, s(x)) \partial_l G^\pm(x, s(x)) - G^\pm(x, s(x)) \partial_l \psi_1(x, s(x))] n_l(x) dx \end{aligned} \quad (2.19)$$

Equation (2.19) is a very important result, as it provides the key relationship between what occurs on the surface and what occurs at $z = H$. It is appropriate at this point to make an important comment on notation, which is somewhat ambiguous in Equation (2.19). The term $\partial_3 G^\pm(x, H)$ should be taken to mean $\partial_3 G^\pm(x, z)|_{z=H}$, and the other three derivative terms should be interpreted similarly. This style of notation will be used throughout the thesis.

To continue the analysis, we use Equations (1.14), (2.1), and (2.16) to write

$$\begin{aligned} \psi_1(x, H) &= \psi^0(x, H) + \int_{-\infty}^{\infty} A(\mu) e^{ik_1(\mu x + mH)} d\mu \\ \partial_3 \psi_1(x, H) &= \partial_3 \psi^0(x, H) + ik_1 \int_{-\infty}^{\infty} mA(\mu) e^{ik_1(\mu x + mH)} d\mu \\ G^\pm(x, H) &= e^{ik_1(\pm\gamma H - \zeta x)} \\ G^\pm(x, s(x)) &= e^{ik_1(\pm\gamma s(x) - \zeta x)} \\ \partial_3 G^\pm(x, H) &= \pm ik_1 \gamma G^\pm(x, H) \\ n_l \partial_l G^\pm(x, s(x)) &= ik_1(\pm\gamma + s'(x)\zeta) G^\pm(x, s(x)) \end{aligned} \quad (2.20)$$

Also, to simplify notation, we introduce the following new terms:

$$\begin{aligned} \phi_1(x) &= \psi_1(x, s(x)) \\ N_1(x) &= \left(\frac{1}{ik_1}\right) n_l \partial_l \psi_1(x, s(x)) \\ M^0(x, H) &= \left(\frac{1}{ik_1}\right) \partial_3 \psi^0(x, H) \end{aligned} \quad (2.21)$$

Using Equations (2.20) and (2.21), we can express Equation (2.19) as

$$\begin{aligned}
& \int_{-\infty}^{\infty} [\pm\gamma\psi^0(x, H) - M^0(x, H)]e^{ik_1(\pm\gamma H - \zeta x)} dx \\
& + \int_{-\infty}^{\infty} \int_{-\infty}^{\infty} (\pm\gamma - m)A(\mu)e^{ik_1(\pm\gamma H - \zeta x)}e^{ik_1(\mu x + mH)} d\mu dx \\
& = \int_{-\infty}^{\infty} [(\pm\gamma + s'(x)\zeta)\phi_1(x) - N_1(x)]e^{ik_1(\pm\gamma s(x) - \zeta x)} dx
\end{aligned} \tag{2.22}$$

which can be expressed alternatively as

$$\begin{aligned}
& e^{\pm ik_1\gamma H} \int_{-\infty}^{\infty} [\pm\gamma\psi^0(x, H) - M^0(x, H)]e^{-ik_1\zeta x} dx \\
& + \int_{-\infty}^{\infty} (\pm\gamma - m)A(\mu)e^{ik_1(m\pm\gamma)H} \left[\int_{-\infty}^{\infty} e^{ik_1(\mu - \zeta)x} dx \right] d\mu \\
& = \int_{-\infty}^{\infty} [(\pm\gamma + s'(x)\zeta)\phi_1(x) - N_1(x)]e^{ik_1(\pm\gamma s(x) - \zeta x)} dx
\end{aligned} \tag{2.23}$$

We now make use of the identity [3]

$$\int_{-\infty}^{\infty} e^{ik_1(\mu - \zeta)x} dx = \left(\frac{2\pi}{k_1} \right) \delta(\mu - \zeta) \tag{2.24}$$

to obtain

$$\begin{aligned}
& \left(\frac{2\pi}{k_1} \right) (\pm\gamma - \gamma)A(\zeta)e^{ik_1(\gamma\pm\gamma)H} \\
& + e^{\pm ik_1\gamma H} \int_{-\infty}^{\infty} [\pm\gamma\psi^0(x, H) - M^0(x, H)]e^{-ik_1\zeta x} dx \\
& = \int_{-\infty}^{\infty} [(\pm\gamma + s'(x)\zeta)\phi_1(x) - N_1(x)]e^{ik_1(\pm\gamma s(x) - \zeta x)} dx
\end{aligned} \tag{2.25}$$

Since the parameter ζ is simply an arbitrary label for the spectral variable of the auxiliary function G^\pm , it may be replaced everywhere in Equation (2.25) by the parameter μ , without loss of generality. Of course, this mandates the replacement of the parameter γ everywhere with the parameter m . Also realize that Equation (2.25) is actually two equations, because of the “ \pm ” sign. The equation associated with the

positive sign is

$$\begin{aligned} e^{ik_1 mH} \int_{-\infty}^{\infty} [m\psi^0(x, H) - M^0(x, H)]e^{-ik_1 \mu x} dx \\ = \int_{-\infty}^{\infty} [(m + \mu s'(x))\phi_1(x) - N_1(x)]e^{ik_1 (ms(x) - \mu x)} dx \end{aligned} \quad (2.26)$$

and the equation associated with the negative sign is

$$\begin{aligned} e^{-ik_1 mH} \int_{-\infty}^{\infty} [m\psi^0(x, H) + M^0(x, H)]e^{-ik_1 \mu x} dx + \left(\frac{4\pi m}{k_1}\right) A(\mu) \\ = \int_{-\infty}^{\infty} [(m - \mu s'(x))\phi_1(x) + N_1(x)]e^{-ik_1 (ms(x) + \mu x)} dx \end{aligned} \quad (2.27)$$

To further simplify the notation, we introduce

$$F_1(\mu) = e^{ik_1 mH} \int_{-\infty}^{\infty} [m\psi^0(x, H) - M^0(x, H)]e^{-ik_1 \mu x} dx \quad (2.28)$$

and

$$F_2(\mu) = e^{-ik_1 mH} \int_{-\infty}^{\infty} [m\psi^0(x, H) + M^0(x, H)]e^{-ik_1 \mu x} dx \quad (2.29)$$

So, Equations (2.26) and (2.27) become

$$\int_{-\infty}^{\infty} [(m + \mu s'(x))\phi_1(x) - N_1(x)]e^{ik_1 (ms(x) - \mu x)} dx = F_1(\mu) \quad (2.30)$$

and

$$\begin{aligned} A(\mu) = \left(\frac{k_1}{4\pi m}\right) F_2(\mu) \\ + \left(\frac{k_1}{4\pi m}\right) \int_{-\infty}^{\infty} [(m - \mu s'(x))\phi_1(x) + N_1(x)]e^{-ik_1 (ms(x) + \mu x)} dx \end{aligned} \quad (2.31)$$

respectively. In this thesis, only the Dirichlet boundary condition

$$\psi_1(x, s(x)) \equiv 0 \quad (2.32)$$

is considered. So, by Equation (2.21), it is clear that for the Dirichlet problem, we have

$$\phi_1(x) \equiv 0 \quad (2.33)$$

In addition, $F_1(\mu)$ and $F_2(\mu)$ are known functions since they are associated only with the characteristics of the incident field. So, using Equations (1.9), (2.21), (2.28), and (2.29), we obtain the following:

$$F_1(\mu) = \left(\frac{4\pi D\beta}{k_1} \right) \delta(\alpha - \mu) \quad (2.34)$$

and

$$F_2(\mu) \equiv 0 \quad (2.35)$$

Therefore, substituting Equations (2.33) and (2.35) into Equations (2.26) and (2.27) yields the following set of equations for the scattered amplitudes $A(\mu)$ for an arbitrary perfectly-reflecting surface, a plane-wave incident field, and Dirichlet boundary conditions:

$$A(\mu) = \left(\frac{k_1}{4\pi m} \right) \int_{-\infty}^{\infty} e^{-ik_1(ms(x)+\mu x)} N_1(x) dx \quad (2.36)$$

where the unknown boundary value $N_1(x)$ is found by solving

$$\int_{-\infty}^{\infty} e^{ik_1(ms(x)-\mu x)} N_1(x) dx = -F_1(\mu) \quad (2.37)$$

$$F_1(\mu) = \left(\frac{4\pi D\beta}{k_1} \right) \delta(\alpha - \mu) \quad (2.38)$$

It is also important to note that energy must be conserved. Since the surface is perfectly-reflecting, there is no transmitted field. Thus, our energy-conservation equation becomes

$$J_z^0(x, z) + J_z^{sc}(x, z) = 0 \quad (2.39)$$

where J_z^0 and J_z^{sc} represent the z -component of the incident flux density and that of the scattered flux density, respectively. They are defined as

$$J_z^0(x, z) = \rho_1 [\psi^0(x, z) \partial_3 \overline{\psi^0(x, z)} - \overline{\psi^0(x, z)} \partial_3 \psi^0(x, z)] \quad (2.40)$$

$$J_z^{sc}(x, z) = \rho_1 [\psi^{sc}(x, z) \partial_3 \overline{\psi^{sc}(x, z)} - \overline{\psi^{sc}(x, z)} \partial_3 \psi^{sc}(x, z)] \quad (2.41)$$

where the bar notation denotes complex conjugation and the constant ρ_1 is associated with the characteristics of the medium above $s(x)$. In acoustics, ρ_1 represents density, and in electromagnetics, ρ_1 is the permeability for the TE-polarized (i.e. Dirichlet) case, or the dielectric constant for the TM-polarized (i.e. Neumann) case. Recall that this thesis assumes Dirichlet boundary conditions.

Recall also that from Equation (1.9), ψ^0 is given by

$$\psi^0(x, z) = D e^{ik_1(\alpha x - \beta z)} \quad (2.42)$$

Since α and β are both real, it follows that

$$\begin{aligned}\partial_3 \psi^0(x, z) &= -ik_1 \beta D e^{ik_1(\alpha x - \beta z)} \\ \overline{\psi^0(x, z)} &= D e^{-ik_1(\alpha x - \beta z)} \\ \partial_3 \overline{\psi^0(x, z)} &= ik_1 \beta D e^{-ik_1(\alpha x - \beta z)}\end{aligned}\tag{2.43}$$

Substituting Equations (2.42) and (2.43) into Equation (2.40) gives

$$J_z^0(x, z) = i2k_1 \beta D^2 \rho_1\tag{2.44}$$

Next, recall that from Equation (1.10), $\psi^{sc}(x, z)$ is given by

$$\psi^{sc}(x, z) = \int_{-\infty}^{\infty} A(\mu) e^{ik_1(\mu x + mz)} d\mu\tag{2.45}$$

from which it follows that

$$\partial_3 \psi^{sc}(x, z) = ik_1 m \int_{-\infty}^{\infty} A(\mu) e^{ik_1(\mu x + mz)} d\mu\tag{2.46}$$

Since μ is simply the variable of integration in Equation (2.46), and m depends only on μ , then μ and m can be replaced by ζ and γ , respectively. So, Equation (2.46) can be expressed as

$$\psi^{sc}(x, z) = \int_{-\infty}^{\infty} A(\zeta) e^{ik_1(\zeta x + \gamma z)} d\zeta\tag{2.47}$$

and it follows that

$$\overline{\psi^{sc}(x, z)} = \int_{-\infty}^{\infty} \overline{A(\zeta) e^{ik_1(\zeta x + \gamma z)}} d\zeta\tag{2.48}$$

The variable γ can be real or pure imaginary, and ζ is of course always real. Thus,

$$\overline{e^{ik_1(\zeta x + \gamma z)}} = \overline{e^{ik_1 \zeta x} e^{ik_1 \gamma z}} = e^{-ik_1 \zeta x} \overline{e^{ik_1 \gamma z}} \quad (2.49)$$

If γ is real, then

$$\overline{e^{ik_1 \gamma z}} = e^{-ik_1 \gamma z} = e^{-ik_1 \bar{\gamma} z} \quad (2.50)$$

and if γ is imaginary, then

$$\overline{e^{ik_1 \gamma z}} = e^{ik_1 \gamma z} = e^{ik_1 (-\bar{\gamma}) z} = e^{-ik_1 \bar{\gamma} z} \quad (2.51)$$

Hence, Equation (2.48) becomes

$$\overline{\psi^{sc}(x, z)} = \int_{-\infty}^{\infty} \overline{A(\zeta)} e^{-ik_1(\zeta x + \bar{\gamma} z)} d\zeta \quad (2.52)$$

It follows that

$$\partial_3 \overline{\psi^{sc}(x, z)} = -ik_1 \bar{\gamma} \int_{-\infty}^{\infty} \overline{A(\zeta)} e^{-ik_1(\zeta x + \bar{\gamma} z)} d\zeta \quad (2.53)$$

Substituting the expressions from Equations (2.45), (2.46), (2.52), and (2.53) into Equation (2.41) yields

$$J_z^{sc}(x, z) = -ik_1 \rho_1 \int_{-\infty}^{\infty} \int_{-\infty}^{\infty} A(\mu) \overline{A(\zeta)} (m + \bar{\gamma}) e^{ik_1[(\mu - \zeta)x + (m - \gamma)z]} d\mu d\zeta . \quad (2.54)$$

Therefore, Equations (2.44) and (2.54) combine with Equation (2.39) to produce

$$\int_{-\infty}^{\infty} \int_{-\infty}^{\infty} A(\mu) \overline{A(\zeta)} (m + \bar{\gamma}) e^{ik_1[(\mu - \zeta)x + (m - \gamma)z]} d\mu d\zeta = 2\beta D^2 . \quad (2.55)$$

Certainly, conservation of energy holds true for all points on the line $z = H$. Therefore, we can substitute $z = H$ into Equation (2.55), then integrate both sides from $x = -\frac{\Lambda}{2}$ to $x = \frac{\Lambda}{2}$, and then finally take the limit as Λ approaches infinity, in order to include the entire line $z = H$. This results in the following, after changing the order of integration on the left-hand side:

$$\int_{-\infty}^{\infty} \int_{-\infty}^{\infty} A(\mu) \overline{A(\zeta)} (m + \overline{\gamma}) e^{ik_1(m-\gamma)z} \left[\int_{-\frac{\Lambda}{2}}^{\frac{\Lambda}{2}} e^{ik_1(\mu-\zeta)x} dx \right] d\mu d\zeta = 2\beta\Lambda D^2 \quad (2.56)$$

In order to define an incident flux per unit length on the surface, we normalize using

$$D = \sqrt{\frac{2\pi}{k_1\Lambda}} \quad (2.57)$$

Hence, the right-hand side of Equation (2.56) becomes $\frac{4\pi\beta}{k_1}$. We now take the limit as Λ approaches infinity, and use Equation (2.24) to obtain

$$\left(\frac{2\pi}{k_1}\right) \int_{-\infty}^{\infty} A(\mu) \overline{A(\mu)} (m + \overline{m}) d\mu = \frac{4\pi\beta}{k_1} \quad (2.58)$$

From this comes the following energy-conservation equation:

$$\frac{1}{\beta} \int_{-1}^1 |A(\mu)|^2 m d\mu = 1 \quad (2.59)$$

The limits of integration in Equation (2.59) have been truncated since Equation (1.11) implies that $\mathcal{F}\{m\}$ is non-zero only for $|\mu| \leq 1$. If one works out a solution for the scattered amplitudes, and Equation (2.59) fails to hold, then the solution is inaccurate to some degree. Equation (2.38) - (2.40) and (2.59) can be found in DeSanto's paper

[4].

Our next step is to modify Equations (2.36) - (2.38) by making the assumption that the surface is periodic, and to derive an analogous energy-conservation equation for the periodic case.

Chapter 3

INTEGRAL EQUATIONS FOR PERIODIC SURFACES

Often in practice, surfaces arise that are nearly periodic in the domain of interest, so that one may represent them approximately by using surface functions $s(x)$ that are truly periodic. Since Equations (2.36) - (2.38) and Equation (2.59) were all developed assuming a surface of infinite length, we note that an infinitely-long periodic surface function can be constructed by approximating a long finite periodic surface function with its periodic extension.

We shall continue working with the assumptions that our surface is perfectly-reflecting, the incident field consists of a single plane wave, and Dirichlet boundary conditions apply, and we shall now include the additional assumption that $s(x)$ is a periodic function. Although Equation (1.10) indicates that the spectrum of scattered waves is generally continuous, this chapter illustrates that the spectrum associated with a periodic surface is discrete. The purpose of this chapter is to derive the equations for the scattered amplitudes relating to periodic surfaces, from the equations relating to arbitrary surfaces in DeSanto's paper [4]. The energy conservation equation for periodic surfaces is also developed here. The results, which involve Bessel functions in the case of a sinusoidal surface, can be found in some of DeSanto's earlier work (e.g. [5], [6]).

Assume $s(x)$ is periodic with period L . By the definition of periodicity,

$$s\left(x - \frac{L}{2}\right) = s\left(x + \frac{L}{2}\right) \quad \forall x \in \mathfrak{R} \quad (3.1)$$

Equation (2.21) states that the function $N_1(x)$ represents a scaled version of the normal derivative of the field on the surface. In addition, $N_1(x)$ is periodic up to a phase lag, meaning that it can be written in the form

$$N_1(x) = e^{ik_1 \alpha x B(x)} \quad (3.2)$$

where $B(x)$ is periodic with period L . Since $B(x)$ is periodic, we have

$$B(x) = B(x + L) \quad (3.3)$$

and thus, from Equations (3.2) and (3.3), we establish the Floquet boundary condition

$$N_1(x + L) = e^{ik_1 \alpha L} N_1(x) \quad (3.4)$$

So, we begin by expressing Equations (2.37) and (2.36), respectively, as infinite sums of integrals over finite domains:

$$\sum_{\kappa=-\infty}^{\infty} \int_{\frac{L}{2}(2\kappa-1)}^{\frac{L}{2}(2\kappa+1)} e^{ik_1(ms(x)-\mu x)} N_1(x) dx = -F_1(\mu) \quad (3.5)$$

$$A(\mu) = \left(\frac{k_1}{4\pi m} \right) \sum_{\kappa=-\infty}^{\infty} \int_{\frac{L}{2}(2\kappa-1)}^{\frac{L}{2}(2\kappa+1)} e^{-ik_1(ms(x)+\mu x)} N_1(x) dx \quad (3.6)$$

We implement a change in the variable of integration by introducing y such that

$$\begin{aligned} y &= x + \kappa L \\ x &= y - \kappa L \\ dx &= dy \end{aligned} \quad (3.7)$$

So using Equations (3.1), (3.4), and (3.7), we write Equations (3.5) and (3.6), respectively, as

$$\sum_{\kappa=-\infty}^{\infty} \int_{-\frac{L}{2}}^{\frac{L}{2}} e^{ik_1(ms(y)-\mu y)} e^{ik_1\kappa L(\mu-\alpha)} N_1(y) dy = -F_1(\mu) \quad (3.8)$$

and

$$A(\mu) = \left(\frac{k_1}{4\pi m} \right) \sum_{\kappa=-\infty}^{\infty} \int_{-\frac{L}{2}}^{\frac{L}{2}} e^{ik_1(ms(y)+\mu y)} e^{ik_1\kappa L(\mu-\alpha)} N_1(y) dy \quad (3.9)$$

We may change the variable of integration from y to x without loss of generality, and we may also extract from the integral the term that is independent of the variable of integration. Such manipulations, along with the use of Equation (2.38), provide

$$\left[\sum_{\kappa=-\infty}^{\infty} e^{ik_1\kappa L(\mu-\alpha)} \right] \int_{-\frac{L}{2}}^{\frac{L}{2}} e^{ik_1(ms(x)-\mu x)} N_1(x) dx = - \left(\frac{4\pi D\beta}{k_1} \right) \delta(\alpha - \mu) \quad (3.10)$$

$$A(\mu) = \left(\frac{k_1}{4\pi m} \right) \left[\sum_{\kappa=-\infty}^{\infty} e^{ik_1\kappa L(\mu-\alpha)} \right] \int_{-\frac{L}{2}}^{\frac{L}{2}} e^{-ik_1(ms(x)+\mu x)} N_1(x) dx \quad (3.11)$$

At this point, we use the identity

$$\sum_{\kappa=-\infty}^{\infty} e^{i\kappa\tau} = 2\pi \sum_{p=-\infty}^{\infty} \delta(\tau - 2\pi p) \quad (3.12)$$

which can be derived from Equation (2.24). So, letting $\tau = k_1 L(\mu - \alpha)$, we obtain

$$\begin{aligned} \sum_{\kappa=-\infty}^{\infty} e^{ik_1\kappa L(\mu-\alpha)} &= 2\pi \sum_{p=-\infty}^{\infty} \delta(k_1 L(\mu - \alpha) - 2\pi p) \\ &= \left(\frac{2\pi}{k_1 L} \right) \sum_{p=-\infty}^{\infty} \delta\left(\mu - \left[\alpha + \frac{2\pi p}{k_1 L}\right]\right) \end{aligned} \quad (3.13)$$

We now adopt the notation

$$\mu_p = \alpha + \frac{2\pi p}{k_1 L} = \alpha + p \left(\frac{\lambda_1}{L} \right) \quad (3.14)$$

which is known as the the grating equation, and will be examined later in the derivation. So, substituting Equations (3.13) and (3.14) into Equations (3.10) and (3.11) results in

$$\left[\sum_{p=-\infty}^{\infty} \delta(\mu - \mu_p) \right] \int_{-\frac{L}{2}}^{\frac{L}{2}} e^{ik_1(ms(x)-\mu x)} N_1(x) dx = -2D\beta L\delta(\alpha - \mu) \quad (3.15)$$

and

$$A(\mu) = \left(\frac{1}{2mL} \right) \left[\sum_{p=-\infty}^{\infty} \delta(\mu - \mu_p) \right] \int_{-\frac{L}{2}}^{\frac{L}{2}} e^{-ik_1(ms(x)+\mu x)} N_1(x) dx \quad (3.16)$$

Next, we introduce a very small parameter ε such that $0 < \varepsilon < \frac{\lambda}{L}$. Then, for some integer ν , we integrate both sides of Equations (3.15) and (3.16), over μ from $\mu = (\mu_\nu - \varepsilon)$ to $\mu = (\mu_\nu + \varepsilon)$, and then take the limit as $\varepsilon \rightarrow 0$. Every term on the left-hand side of Equation (3.15) will vanish except for the term associated with $p = \nu$. The term on the right-hand side of Equation (3.15) vanishes unless $\alpha = \mu_\nu$, which, following Equation (3.14), only occurs when $\nu = 0$. Since ν can take on the value of any integer, Equation (3.15) becomes

$$\int_{-\frac{L}{2}}^{\frac{L}{2}} e^{ik_1(m_\nu s(x)-\mu_\nu x)} N_1(x) dx = \begin{cases} -2Dm_0L & \nu = 0 \\ 0 & \nu \neq 0 \end{cases} \quad (3.17)$$

which can be written as

$$\int_{-\frac{L}{2}}^{\frac{L}{2}} e^{ik_1(m_\nu s(x)-\mu_\nu x)} N_1(x) dx = -2Dm_0L\delta_{\nu 0} \quad \nu = 0, \pm 1, \pm 2, \dots \quad (3.18)$$

Since $m_0 = \beta$, the term m_0 on the right-hand side of Equation (3.18) can be replaced by β . After performing the same integration and taking the limit as $\varepsilon \rightarrow 0$, the

left-hand side of Equation (3.16) simply becomes $A(\mu_\nu)$, and every term on the right-hand side of Equation (3.16) vanishes except for the term associated with $p = \nu$. This yields

$$A_\nu = A(\mu_\nu) = \left(\frac{1}{2m_\nu L} \right) \int_{-\frac{L}{2}}^{\frac{L}{2}} e^{-ik_1(m_\nu s(x) + \mu_\nu x)} N_1(x) dx \quad \nu = 0, \pm 1, \pm 2, \dots \quad (3.19)$$

Since the scattered field is now comprised of a discrete spectrum of plane waves, we replace Equation (1.10) with

$$\psi^{sc}(x, z) = \sum_{\nu=-\infty}^{\infty} A_\nu e^{ik_1(\mu_\nu x + m_\nu z)} \quad (3.20)$$

It should be noted that Bragg indices ν for which $|\mu_\nu| < 1$ are associated with upgoing scattered waves, where $\mu_\nu = \sin[(\theta_{sc})_\nu]$ and $m_\nu = \cos[(\theta_{sc})_\nu]$. In addition, Bragg indices for which $|\mu_\nu| > 1$ are associated with nonradiating surface waves, and Bragg indices for which $|\mu_\nu| = 1$ are associated with plane waves which are “scattered” horizontally, thus never entering region A .

Also, since the surface is periodic, the scattered field is Floquet periodic, and therefore, the ratio $\frac{\psi^{sc}}{\psi^0}$ is periodic. Thus,

$$\left. \frac{\psi^{sc}}{\psi^0} \right|_{x=x_0} = \left. \frac{\psi^{sc}}{\psi^0} \right|_{x=x_0+L} \quad (3.21)$$

So, substituting Equations (1.9) and (3.20) into Equation (3.21) tells us that the following must hold:

$$e^{i\left(\frac{2\pi}{\lambda_1}\right)(\mu_\nu - \alpha)L} = 1 \quad (3.22)$$

So, the term $\left(\frac{L}{\lambda_1}\right)(\mu_\nu - \alpha)$ must be an integer. Therefore, we obtain the aforementioned

grating equation

$$\mu_\nu = \alpha + \nu \left(\frac{\lambda_1}{L} \right) \quad \nu = 0, \pm 1, \pm 2, \dots \quad (3.23)$$

Equation (3.23) is a form for Bragg's Law, which is often associated with atomic beam scattering from crystal lattices [7]. The index ν in Equations (3.18), (3.19), and (3.23) is known as the Bragg index, and when $|\mu_\nu| < 1$, $(\theta_{sc})_\nu = \sin^{-1}(\mu_\nu)$ is known as the Bragg scattered angle of order ν . In addition, since the spectrum of scattered waves is now discrete, the energy-conservation requirement given by Equation (2.59) is modified to become

$$\sum_{\nu \text{ s.t. } |\mu_\nu| < 1} \left(\frac{m_\nu}{\beta} \right) |A_\nu|^2 = 1 \quad (3.24)$$

Therefore, we summarize our findings as such:

For plane-wave incidence onto a perfectly-reflecting periodic surface given by $z = s(x)$, and applying Dirichlet boundary conditions, these equations are exactly valid above the highest surface excursion:

$$\psi(x, z) = D e^{ik_1(\alpha x - \beta z)} + \sum_{\nu=-\infty}^{\infty} A_\nu e^{ik_1(\mu_\nu x + m_\nu z)} \quad (3.25)$$

The scattered amplitudes are such that for $\nu = 0, \pm 1, \pm 2, \dots$:

$$A_\nu = \left(\frac{1}{2m_\nu L} \right) \int_{-\frac{L}{2}}^{\frac{L}{2}} e^{-ik_1(m_\nu s(x) + \mu_\nu x)} N_1(x) dx \quad (3.26)$$

where $N_1(x)$ is the solution to the first-kind integral equation

$$\int_{-\frac{L}{2}}^{\frac{L}{2}} e^{ik_1(m_\nu s(x) - \mu_\nu x)} N_1(x) dx = -2D\beta L\delta_{\nu 0} \quad (3.27)$$

Also,

$$\mu_\nu = \alpha + \nu \left(\frac{\lambda_1}{L} \right) \quad \nu = 0, \pm 1, \pm 2, \dots \quad (3.28)$$

$$m_\nu = \begin{cases} +\sqrt{1 - \mu_\nu^2} & |\mu_\nu| \leq 1 \\ +i\sqrt{\mu_\nu^2 - 1} & 1 \leq |\mu_\nu| \end{cases} \quad (3.29)$$

$$\begin{aligned} \alpha &= \sin(\theta_{inc}) & \beta &= \cos(\theta_{inc}) \\ \mu_\nu &= \sin[(\theta_{sc})_\nu] & m_\nu &= \cos[(\theta_{sc})_\nu] \quad \nu \text{ s.t. } |\mu_\nu| < 1 \end{aligned} \quad (3.30)$$

The sign convention for θ_{inc} and each θ_{sc} is in accordance with Figure (1.2).

The energy-conservation equation is

$$\sum_{\nu \text{ s.t. } |\mu_\nu| < 1} \left(\frac{m_\nu}{\beta} \right) |A_\nu|^2 = 1 \quad (3.31)$$

Note that the kernel of the integral equation given by Equation (3.27) is in the mixed (discrete) spectral-coordinate form.

Numerical solutions have been generated for the specific case of a sinusoidal surface, using a physical optics approximation [8]-[12], and other results have been obtained by direct numerical solution of integral equations in coordinate space [13], [14]. However, to the best of the author's knowledge, no numerical solutions have ever been generated using a direct discretization of Equations (3.25) - (3.31). The remain-

der of this thesis is dedicated to exploring this new approach, which will hopefully lead to solutions for arbitrary period surfaces.

Chapter 4

DISCRETIZATION OF THE INTEGRAL EQUATION

We continue working with the assumptions that the surface is perfectly-reflecting and periodic, the incident field is a plane wave, and Dirichlet boundary conditions apply, so as to maintain the applicability of Equations (3.25) - (3.31). In particular, Equation (3.27) will be the focus of this chapter because once it has been solved for $N_1(x)$, the scattered amplitudes can be obtained directly from Equation (3.26). Because Equations (3.27) - (3.29) will be referred to quite frequently in this chapter, we restate them here for convenience.

$$\int_{-\frac{L}{2}}^{\frac{L}{2}} e^{ik_1(m_\nu s(x) - \mu_\nu x)} N_1(x) dx = -2D\beta L\delta_{\nu 0} \quad (4.1)$$

where

$$\mu_\nu = \alpha + \nu \left(\frac{\lambda_1}{L} \right) \quad (4.2)$$

and

$$m_\nu = \begin{cases} +\sqrt{1 - \mu_\nu^2} & |\mu_\nu| \leq 1 \\ +i\sqrt{\mu_\nu^2 - 1} & 1 \leq |\mu_\nu| \end{cases} \quad (4.3)$$

for $\nu = 0, \pm 1, \pm 2, \dots$

Equation (4.1) is a countably-infinite system of equations, with the function $N_1(x)$ serving as the unknown in all of them; hence, $N_1(x)$ must satisfy every equation in the system. This system of equations is somewhat akin to a single Fredholm integral equation of the first kind. In fact, perhaps it can be thought of as a first-kind integral equation [15] where the kernel is a function of one variable over a continuous

(coordinate) domain and one variable over a discrete (spectral) domain.

A common technique employed in numerically solving a “standard” first-kind integral equation (i.e. one in which the domains associated with both independent variables are continuous) is that which involves discretizing the variable of integration, as in a scheme for numerical integration, then discretizing the other independent variable. This serves to express the problem in matrix-vector form, where the unknown vector represents the values of the unknown function in the integral equation at the spatial mesh points. This seems to be an ideal approach for solving Equation (4.1) since the spectral variable has been discretized already. In fact, the mesh points associated with that variable are determined directly from Equation (4.2).

We proceed by discretizing the spatial variable x over the interval from $x = -\frac{L}{2}$ to $x = \frac{L}{2}$. The grid points shall be denoted as x_1, x_2, \dots, x_n , and we shall impose the restriction that n is odd, the reason for which will become apparent shortly. Also, the mesh is to be labelled such that

$$-\frac{L}{2} = x_1 < x_2 < \dots < x_{n-1} < x_n = \frac{L}{2} \quad (4.4)$$

We proceed now to derive a “generalized” form of Simpson’s Rule for numerical integration [16]. The generalization lies in the fact that we will not restrict ourselves to working with a uniform mesh.

Consider the integrand on the left-hand side of Equation (4.1). For simplicity, we denote it as

$$y(x) = y(x; \mu_\nu) = k(\mu_\nu, x)N_1(x) \quad \nu \in \{0, \pm 1, \pm 2, \dots\} \quad (4.5)$$

where

$$k(\mu_\nu, x) = e^{ik_1(m_\nu s(x) - \mu_\nu x)} \quad \nu = 0, \pm 1, \pm 2, \dots \quad (4.6)$$

In Equation (4.5), we treat μ_ν as a parameter, and it will occasionally be convenient in the upcoming discussion to suppress it from the notation. We can write Equation (4.1) as the following for $\nu = 0, \pm 1, \pm 2, \dots$:

$$\int_{-\frac{L}{2}}^{\frac{L}{2}} k(\mu_\nu, x) N_1(x) dx = \int_{-\frac{L}{2}}^{\frac{L}{2}} y(x; \mu_\nu) dx = -2D\beta L \delta_{\nu 0} \quad (4.7)$$

We denote the function values of the integrand of Equation (4.7) at the mesh points as

$$y_j = y(x_j) \quad j = 1, 2, \dots, n \quad (4.8)$$

where y_j is tacitly assumed to be associated with some Bragg index ν .

With this in mind, we turn our attention to the region of the spatial domain given by $x_1 \leq x \leq x_3$. In this region, the curve $y(x)$ must pass through the points (x_1, y_1) , (x_2, y_2) , and (x_3, y_3) . There exists a unique parabola which also passes through these three points, and it will be used to approximate $y(x)$ over this domain. This parabola can be represented by the following Lagrange interpolating quadratic [17]:

$$\begin{aligned} \hat{y}(x) = & \left[\frac{(x - x_2)(x - x_3)}{(x_1 - x_2)(x_1 - x_3)} \right] y_1 \\ & + \left[\frac{(x - x_1)(x - x_3)}{(x_2 - x_1)(x_2 - x_3)} \right] y_2 \\ & + \left[\frac{(x - x_1)(x - x_2)}{(x_3 - x_1)(x_3 - x_2)} \right] y_3 \end{aligned} \quad (4.9)$$

So, we make the approximation

$$\int_{x_1}^{x_3} y(x)dx \approx \int_{x_1}^{x_3} \hat{y}(x)dx \quad (4.10)$$

For a general mesh, the error involved in this approximation is on the order of the cube of the largest interval length in the mesh.

We proceed to integrate the interpolating quadratic, using Equation (4.9).

$$\begin{aligned} \int_{x_1}^{x_3} \hat{y}(x)dx &= \frac{y_1}{(x_2 - x_1)(x_3 - x_1)} \int_{x_1}^{x_3} (x - x_2)(x - x_3)dx \\ &\quad - \frac{y_2}{(x_2 - x_1)(x_3 - x_2)} \int_{x_1}^{x_3} (x - x_1)(x - x_3)dx \\ &\quad + \frac{y_3}{(x_3 - x_1)(x_3 - x_2)} \int_{x_1}^{x_3} (x - x_1)(x - x_2)dx \end{aligned} \quad (4.11)$$

Performing each integration by parts gives

$$\begin{aligned} \int_{x_1}^{x_3} \hat{y}(x)dx &= \left[\frac{(x_3 - x_1)}{6(x_2 - x_1)} \right] [2(x_2 - x_1) - (x_3 - x_2)]y_1 \\ &\quad + \left[\frac{(x_3 - x_1)^3}{6(x_2 - x_1)(x_3 - x_2)} \right] y_2 \\ &\quad + \left[\frac{(x_3 - x_1)}{6(x_3 - x_2)} \right] [2(x_3 - x_2) - (x_2 - x_1)]y_3 \end{aligned} \quad (4.12)$$

Recall that we have chosen n to be odd, and the reason for this now becomes evident. The analysis of the region $x_1 \leq x \leq x_3$ which resulted in Equation (4.12) can be applied to any region $x_{2k-1} \leq x \leq x_{2k+1}$, $k \in \{1, 2, \dots, (\frac{n-1}{2})\}$. Thus, this equation holds for any such k , with x_{2k-1} replacing x_1 , x_{2k} replacing x_2 , and x_{2k+1} replacing

x_3 , and the general expression becomes

$$\int_{x_{2k-1}}^{x_{2k+1}} \hat{y}(x) dx = A_{2k} y_{2k-1} + B_{2k} y_{2k} + C_{2k} y_{2k+1} \quad k \in \left\{ 1, 2, \dots, \frac{(n-1)}{2} \right\}, \quad (4.13)$$

where

$$A_{2k} = \left[\frac{(x_{2k+1} - x_{2k-1})}{6(x_{2k} - x_{2k-1})} \right] [2(x_{2k} - x_{2k-1}) - (x_{2k+1} - x_{2k})] \quad (4.14)$$

$$B_{2k} = \left[\frac{(x_{2k+1} - x_{2k-1})^3}{6(x_{2k} - x_{2k-1})(x_{2k+1} - x_{2k})} \right] \quad (4.15)$$

$$C_{2k} = \left[\frac{(x_{2k+1} - x_{2k-1})}{6(x_{2k+1} - x_{2k})} \right] [2(x_{2k+1} - x_{2k}) - (x_{2k} - x_{2k-1})] \quad (4.16)$$

We now consider the entire domain of x , given by $-\frac{L}{2} \leq x \leq \frac{L}{2}$. From Equations (4.4) and (4.10), we have

$$\int_{-\frac{L}{2}}^{\frac{L}{2}} y(x) dx \approx \sum_{k=1}^{\left(\frac{n-1}{2}\right)} \int_{x_{2k-1}}^{x_{2k+1}} \hat{y}(x) dx \quad (4.17)$$

where the curve $y(x)$ over the entire domain of x has been replaced with a set of $\left(\frac{n-1}{2}\right)$ piecewise quadratics over that same domain. It follows from Equation (4.13) that

$$\begin{aligned} \int_{-\frac{L}{2}}^{\frac{L}{2}} y(x) dx &\approx A_2 y_1 + B_2 y_2 + C_2 y_3 \\ &\quad + A_4 y_3 + B_4 y_4 + C_4 y_5 \\ &\quad \vdots \\ &\quad + A_{n-1} y_{n-2} + B_{n-1} y_{n-1} + C_{n-1} y_n \end{aligned} \quad (4.18)$$

Thus, combining Equations (4.5) - (4.8) and (4.18), we obtain the following discretized approximation:

$$\sum_{j=1}^n w_j k(\mu_\nu, x_j) N_1(x_j) = -2D\beta L \delta_{\nu 0} \quad \nu = 0, \pm 1, \pm 2, \dots \quad (4.19)$$

where

$$k(\mu_\nu, x_j) = e^{ik_1(m_\nu s(x_j) - \mu_\nu x_j)} \quad \begin{array}{l} \nu = 0, \pm 1, \pm 2, \dots \\ j = 1, 2, \dots, n \end{array} \quad (4.20)$$

and

$$w_j = \begin{cases} A_2 & j = 1 \\ B_j & j \text{ even} \\ (A_{j+1} + C_{j-1}) & j \text{ odd, } 1 < j < n \\ C_{n-1} & j = n \end{cases} \quad (4.21)$$

We are almost ready to formulate our complete discretized representation for the numerical solution of $N_1(x)$. However, notice that since there are infinitely-many Bragg indices, our system is infinitely large. Therefore, we must select a finite sample set of Bragg indices to work with, and for the sake of constructing a square system, we select a sample set of n such indices. Since we are ultimately interested in the scattered amplitudes, the sample set should include all Bragg indices associated with scattered waves (i.e. all ν such that $|\mu_\nu| < 1$).

Each Bragg index accounted for in the spectral sample set will correspond to a row in our matrix, and the rows are to be labelled as $i = 1, 2, \dots, n$. We require a rule of correspondence between the Bragg indices and the rows of the matrix. Thus, we let the Bragg index associated with row i of the matrix be denoted by

$$\nu_i \quad i = 1, 2, \dots, n \quad (4.22)$$

where

$$\begin{aligned}\nu_2 &= \nu_1 + 1 \\ \nu_i &= \nu_{i-1} + 1 \quad i = 2, 3, \dots, n\end{aligned}\tag{4.23}$$

We label the corresponding values of μ and m in the sample set as

$$\begin{aligned}\xi_i &= \mu_{(\nu_i)} \\ \eta_i &= m_{(\nu_i)} \quad i = 1, 2, \dots, n\end{aligned}\tag{4.24}$$

and we also assign

$$K_{ij}^+ = k(\mu_{(\nu_i)}, x_j) = k(\xi_i, x_j)\tag{4.25}$$

$$f_i = -2D\beta L\delta_{(\nu_i)0}\tag{4.26}$$

$$N_{1j} = N_1(x_j)\tag{4.27}$$

Thus, we may now represent our finite sample set of size n from the infinitely-large system given by Equation (4.19) as

$$\sum_{j=1}^n w_j K_{ij}^+ N_{1j} = f_i \quad i = 1, 2, \dots, n\tag{4.28}$$

Equation (4.28) can be written in matrix-vector form, with the unknown vector containing the values of $N_1(x)$ at the spatial mesh points. The following provides a summary of the discretized problem for $N_1(x)$.

Solve the following for \vec{N}_1 :

$$X\vec{N}_1 = \vec{f} \quad , \quad (4.29)$$

where

$$X_{ij} = w_j K_{ij}^+ \quad (4.30)$$

$$K_{ij}^+ = e^{ik_1(\eta_i s(x_j) - \xi_i x_j)} \quad (4.31)$$

$$\xi_i = \alpha + \nu_i \left(\frac{\lambda_1}{L} \right) \quad (4.32)$$

$$\eta_i = \begin{cases} +\sqrt{1 - \xi_i^2} & |\xi_i| \leq 1 \\ +i\sqrt{\xi_i^2 - 1} & 1 \leq |\xi_i| \end{cases} \quad (4.33)$$

$$w_j = \begin{cases} A_2 & j = 1 \\ B_j & j \text{ even} \\ (A_{j+1} + C_{j-1}) & j \text{ odd, } 1 < j < n \\ C_{n-1} & j = n \end{cases} \quad (4.34)$$

$$A_{2k} = \left[\frac{(x_{2k+1} - x_{2k-1})}{6(x_{2k} - x_{2k-1})} \right] [2(x_{2k} - x_{2k-1}) - (x_{2k+1} - x_{2k})] \quad (4.35)$$

$$B_{2k} = \left[\frac{(x_{2k+1} - x_{2k-1})^3}{6(x_{2k} - x_{2k-1})(x_{2k+1} - x_{2k})} \right] \quad (4.36)$$

$$C_{2k} = \left[\frac{(x_{2k+1} - x_{2k-1})}{6(x_{2k+1} - x_{2k})} \right] [2(x_{2k+1} - x_{2k}) - (x_{2k} - x_{2k-1})] \quad (4.37)$$

$$f_i = -2D\beta L\delta_{(\nu_i)0} \quad (4.38)$$

$$N_{1_i} = N_1(x_i) \quad (4.39)$$

$$i = \begin{cases} 1, 2, \dots, n & i \text{ is a subscript} \\ \sqrt{-1} & i \text{ is not a subscript} \end{cases} \quad (4.40)$$

$$j = 1, 2, \dots, n$$

$$k = 1, 2, \dots, \left(\frac{n-1}{2}\right)$$

All that remains for the posing of Equation (4.29) are the actual mesh values ξ_i and x_j , which will be discussed in the next chapter.

Chapter 5

DRIVER FOR NUMERICAL SOLUTION

This chapter serves to complete the derivation of the FORTRAN code for obtaining a numerical solution for the scattered amplitudes. We continue to assume a perfectly-reflecting periodic surface, plane-wave incidence, and Dirichlet boundary conditions. The next step is to select the mesh points for both the spatial and spectral independent variables, which provides the remainder of the information needed to formulate Equation (4.29). Once that has been accomplished, we implement a method for solving $X\vec{N}_1 = \vec{f}$ for the unknown vector \vec{N}_1 , which we subsequently use to directly calculate the desired scattered amplitudes. Provisions for implementing the energy-conservation check in Equation (3.31) are also discussed here.

In order to simplify the discussion, we shall, at this point, impose that all length measurements be expressed in units of wavelength. In other words,

$$\lambda_1 = 1 \tag{5.1}$$

and it follows from Equation (1.6) that

$$k_1 = 2\pi \tag{5.2}$$

So, we begin by considering the discretization of the spectral variable. Much of the

analysis is governed by Equation (4.32), which is restated here with $\lambda_1 = 1$:

$$\xi_i = \alpha + \nu_i \left(\frac{1}{L} \right) \quad i = 1, 2, \dots, n \quad (5.3)$$

where L is now expressed in wavelengths. Recall that our sample set of spectral values must include all values of ξ_i such that $|\xi_i| < 1$, in order to account for all possible scattered waves. So, we search for all i such that

$$-1 < \alpha + \nu_i \left(\frac{1}{L} \right) < 1 \quad (5.4)$$

Such values of i are those which satisfy

$$-L(1 + \alpha) < \nu_i < L(1 - \alpha) \quad (5.5)$$

Normal incidence is defined by $\alpha = 0$ and is represented physically by the orientation of the incident ray being perpendicular to the x -axis and parallel to the z -axis. Assuming normal incidence, Equation (5.5) becomes

$$-L < \nu_i < L \quad (5.6)$$

which indicates that the number of integer values of i which satisfy this condition is approximately $2L$. It is interesting to note that if L is slightly greater than an integer, then the number of values of i satisfying Equation (5.6) is approximately $(2L + 1)$, whereas if L is equal to or slightly less than an integer, then the number of values of i that apply is only approximately $(2L - 1)$.

Since the increment between values of ξ_i for a given L is independent of α , then the number of values of i for which Equation (5.5) holds is approximately $2L$,

regardless of α . However, just as the exact number of values can be affected by slight changes in L , the exact number can also be affected by slight changes in α . Consider some fixed L . A case could arise where for one value of α , there is some ν_i which barely satisfies Equation (5.5). In this case, a slightly different α could cause that ν_i to fall out of range.

Clearly, we must choose our sample size n to be at least as large as the minimum number of i values which satisfy Equation (5.5); otherwise, there will be values of ξ associated with scattered waves that are not included in the sample set. By taking n to be larger than that minimum number, we are simply adding equations to our system which correspond to nonradiating surface waves. Such equations are associated with $|\xi_i| \geq 1$ (i.e. $|\mu_\nu| \geq 1$), and from Equation (4.7), they are part of the infinite system from which we are sampling. There are advantages and disadvantages involved with the inclusion of the $|\xi_i| \geq 1$ equations, which will be discussed later.

Once a value of n has been selected that is known to be large enough to include all $|\xi_i| < 1$ equations (i.e. all equations associated with scattered waves), then the next step is to design the sample set so as to ensure that they are, in fact, all included. Figure (5.1) assists us in this matter.

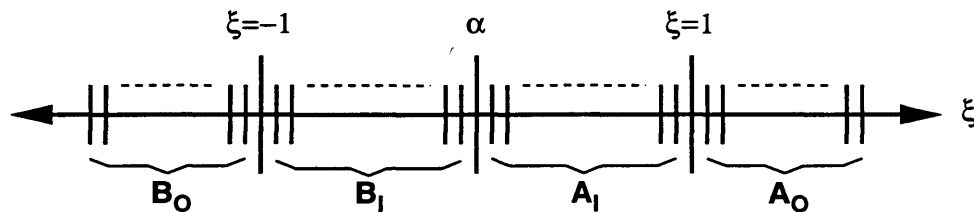


FIG. 5.1. Location of Spectral Samples

There will always be one scattered wave associated with $\xi_i = \mu_0 = \alpha$. Subsets

$A_I, A_O, B_I,$ and B_O represent the following:

$$\begin{aligned}
 A_I &\equiv \text{Samples such that } \alpha < \xi_i < 1 \\
 A_O &\equiv \text{Samples such that } 1 \leq \xi_i \\
 B_I &\equiv \text{Samples such that } -1 < \xi_i < \alpha \\
 B_O &\equiv \text{Samples such that } \xi_i \leq -1
 \end{aligned}
 \tag{5.7}$$

Thus, “ A ” and “ B ” denote “above” and “below”, respectively, and the subscripts “ I ” and “ O ” represent whether a sample is “inside” or “outside” the spectrum of upgoing scattered waves. If $\xi_i = 1$, it becomes an element of A_O , and if $\xi_i = -1$, it becomes an element of B_O . Note that often there are physical situations for which there is only one or no Bragg index ν such that $|\mu_\nu| = 1$.

We shall denote the number of elements in each subset with the corresponding lowercase version of the subset name. Thus,

$$n = a_I + a_O + b_I + b_O + 1 \tag{5.8}$$

Next, we use Equation (5.3) and the criterion

$$|\xi_i| < 1 \tag{5.9}$$

to count the number of elements in A_I and B_I . If $n < (a_I + b_I + 1)$, then there are not enough samples to include the entire spectrum of scattered waves, and so n must be increased accordingly.

Assuming n is large enough to suffice, the number of samples associated with

nonradiating surface waves will be

$$(a_O + b_O) = n - (a_I + b_I + 1) \quad (5.10)$$

We shall implement a scheme such that the sample set is centered about the origin. In other words, if $(a_O + b_O)$ is even, we let $a_O = b_O$, and if $(a_O + b_O)$ is odd, we arbitrarily choose to let $(a_O + 1) = b_O$, for the sake of having some convention.

Thus, we have the tools to determine a_I , a_O , b_I , and b_O . Therefore, we now have enough information to determine the relationship between the Bragg indices ν and the row indices i , as alluded to in Equations (4.22) and (4.23). The first row of the matrix X in Equation (4.29) will be associated with the smallest (i.e. “most negative”) element in the subset B_O and the relationship mentioned in Equation (4.23) will apply. So, Equation (4.22) will be stated as

$$\nu_i = i - (b_I + b_O + 1) \quad i = 1, 2, \dots, n \quad (5.11)$$

Next, we move on to the discretization of the spatial variable. Since we approached the problem with a square system in mind, the number of samples in the x grid must equal n , which has been determined already in addressing the requirements of the spectral discretization. Since the length of the x domain is L wavelengths, and we take n samples over this domain, then we are taking $\frac{n}{L}$ samples per wavelength. Recall that the minimum number of samples required to satisfy the criteria for the spectral discretization was approximately $2L$. Thus, the minimum sampling rate in x is approximately 2 samples per wavelength. As one begins to include ξ samples associated with nonradiating surface waves, one begins to increase the sample size n , and therefore begins to increase the number of samples per wavelength in the x

grid. As stated earlier, there are advantages and disadvantages associated with such a strategy, and they will be discussed later.

Since we have n samples to spread over a domain of length L , the issue of how to distribute them arises. One obvious choice is a uniform distribution, but unfortunately, this approach leads to difficulties in many cases, most notably in the case of normal incidence.

Suppose we have normal incidence and we have selected some appropriate n as our sample size. From Equation (5.3) with $\alpha = 0$ representing normal incidence, we see that the set of ξ_i values has the following structure:

$$\xi_i = \nu_i \left(\frac{1}{L} \right) \quad \begin{array}{l} i \in \{\text{a set of consecutive integers}\} \\ \nu_i \in \{\text{a set of consecutive integers}\} \end{array} \quad (5.12)$$

Consider p and q to be elements of the former set of integers, and further assume that

$$\nu_p = -\nu_q \quad (5.13)$$

and that both ν_p and ν_q are even.

Next, consider the n grid points in x to be evenly distributed over $-\frac{L}{2} \leq x \leq \frac{L}{2}$, so that the distance between any two such points is $\left(\frac{L}{n-1}\right)$. Thus, the set of spatial mesh points has the structure

$$x_s = s \left(\frac{L}{n-1} \right) \quad s \in \{\text{a set of consecutive integers}\} \quad (5.14)$$

Now consider the matrix K^+ from Equation (4.31). We select an arbitrary

column $j = s$, and consider rows $i = p$ and $i = q$. From Equation (4.31),

$$K_{ps}^+ = k(\xi_p, x_s) = e^{ik_1\eta_p s(x_s)} e^{-ik_1\xi_p x_s} \quad (5.15)$$

and

$$K_{qs}^+ = k(\xi_q, x_s) = e^{ik_1\eta_q s(x_s)} e^{-ik_1\xi_q x_s} \quad (5.16)$$

So, from Equations (5.12) and (5.13),

$$\xi_p = -\xi_q \quad (5.17)$$

and thus, from Equation (4.33),

$$\eta_p = \eta_q \quad (5.18)$$

Also, from Equations (5.12) and (5.14),

$$\begin{aligned} \xi_p x_s &= \left(\frac{\nu_p s}{n-1} \right) \\ \xi_q x_s &= \left(\frac{\nu_q s}{n-1} \right) \end{aligned} \quad (5.19)$$

Since ν_p , ν_q , and $(n-1)$ are all even integers, s is an integer, and $k_1 = 2\pi$, then

$$\begin{aligned} k_1 \xi_p x_s &\equiv \text{an integral multiple of } 2\pi \\ k_1 \xi_q x_s &\equiv \text{an integral multiple of } 2\pi \end{aligned} \quad (5.20)$$

Therefore, from Equations (5.15), (5.16), (5.18), and (5.20)

$$K_{ps}^+ = K_{qs}^+ \quad (5.21)$$

Since s was taken to be arbitrary, we have rows p and q of matrix K^+ being equal, and hence, K^+ is singular. The procedure of applying the discretization weights w_j in Equation (4.30) does not change this situation, and therefore, the matrix X in Equation (4.29) is singular. Thus, for normal incidence and a uniform spatial mesh, Equation (4.29) is ill-posed.

Since normal incidence is a very common scenario, we must adjust for this problem. The course we shall take is to stagger the mesh so it is not uniform over $-\frac{L}{2} \leq x \leq \frac{L}{2}$. Recall that the uniform distribution involved dividing the region into $(n - 1)$ equal parts. Consider dividing it into $2(n - 1)$ equal parts as in Figure (5.2), which uses $n = 9$ as an example. Here, the distance between tick marks

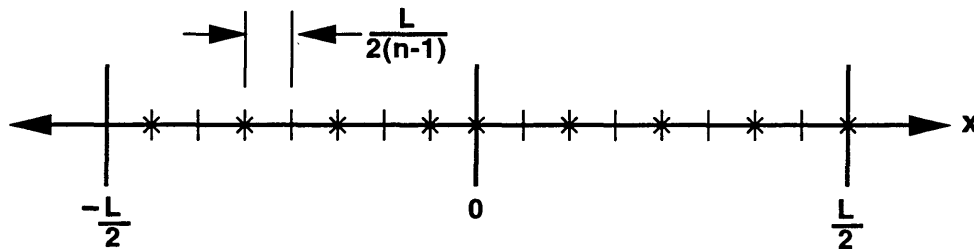


FIG. 5.2. Staggered Sampling for x

is $\frac{L}{2(n-1)}$, and the scheme is to select the odd tick marks for $x < 0$, and the even ones for $x \geq 0$. This staggered effect helps prevent problems that may arise from symmetries in the physical problem, which are quite common. Of course, for any sampling scheme one could contrive a physical setting in which the discretization produces an ill-conditioned system, but this particular scheme seems to handle many commonly-occurring geometries.

To obtain the exact grid point locations for this scheme, we first consider $x < 0$

(i.e. $j \leq \left(\frac{n-1}{2}\right) < \frac{n}{2}$). For such points, we have

$$x_j = (2j - 1) \left[\frac{L}{2(n-1)} \right] - \frac{L}{2} = \frac{(2j - n)L}{2(n-1)} \quad (5.22)$$

For $x \geq 0$, (i.e. $j \geq \left(\frac{n+1}{2}\right) > \frac{n}{2}$), we have

$$x_j = 2 \left(j + \frac{n+1}{2} \right) \left[\frac{L}{2(n-1)} \right] = \frac{(2j - (n+1))L}{2(n-1)} \quad (5.23)$$

So, in summary, the staggered grid scheme for x is given by

$$x_j = \begin{cases} \frac{(2j-n)L}{2(n-1)} & j < \frac{n}{2} \\ \frac{(2j-(n+1))L}{2(n-1)} & \frac{n}{2} < j \end{cases} \quad (5.24)$$

Citing Equations (4.30) - (4.40), (5.11), and (5.24), we now have all the information necessary to formulate the problem as in Equation (4.29), restated here as the square system

$$X\vec{N}_1 = \vec{f} \quad (5.25)$$

However, for some versions of the physical problem, the matrix X may be ill-conditioned, so that the method of solving for \vec{N}_1 becomes an issue. The entries of matrix K^+ , from Equation (4.31), all have a modulus of one, except for the entries in rows associated with i such that $|\xi_i| > 1$. X is formed by applying discretization weights to K^+ , which serves to multiply each column of K^+ by a constant. The resulting $X\vec{N}_1 = \vec{f}$ problem is not readily conducive to iterative methods, which require that the spectral radius of X be less than one, for convergence. The upper bounds on the spectral radii of our matrices X , provided by Gerschgorin's Theorem [18], are not such that they guarantee convergence. Even the use of relaxation techniques, such as

Successive-Over-Relaxation (SOR) [19] seem ill-suited since X is quite far from being diagonally dominant.

The other approach is to find X^{-1} , if it exists, and then to obtain \vec{N}_1 directly by

$$\vec{N}_1 = X^{-1}\vec{f} \quad (5.26)$$

However, in the case of an ill-conditioned X , there is the potential for large inaccuracies in the process of determining X^{-1} . There are two methods that seem best suited for this inversion procedure. The first utilizes the Singular Value Decomposition (SVD) of X [20], and the second makes use of the QR factorization of X [21]. We opt for the SVD approach because the singular values are expressed explicitly as part of this decomposition of X , from which one can gain much information about the effective (i.e. numerical) rank of X . In addition, one may adjust for ill-conditioning by truncating singular values of negligible size, in hopes of maintaining an accurate representation of the problem, with increased stability.

The SVD of X is of the form $X = U\Sigma V^*$, where U and V are unitary matrices, and the singular values of X are the entries of the diagonal matrix Σ . The “*” notation represents taking the conjugate transpose (i.e. Hermitian) of the matrix to which it is applied. If at least one of the singular values of X is truly zero, then X is an exactly singular matrix, and if singular values are near zero, it is considered to be numerically singular, and therefore, severely ill-conditioned.

If X is, in theory, nonsingular, then its inverse is given as $X^{-1} = V\Sigma^{-1}U^*$, where the reciprocals of the singular values of X comprise the entries of the diagonal matrix Σ^{-1} . If X is numerically singular, some entries of Σ^{-1} will be several orders of magnitude larger than others, revealing the ill-conditioned nature of the problem. We can attempt to remove such problems caused by very small singular values.

The pseudo-inverse of X [22] is defined to be $X^+ = V\Sigma^+U^*$, where the entries of the diagonal matrix Σ^+ are given as

$$\Sigma_{ii}^+ = \begin{cases} \frac{1}{\sigma_i} & \epsilon \leq \sigma_i \\ 0 & \sigma_i < \epsilon \end{cases} \quad (5.27)$$

where ϵ is a small parameter selected as the threshold level for numerical singularity. The set $\{\sigma_i\}_{i=1}^n$ is the set of singular values of X , and by convention,

$$0 \leq \sigma_n \leq \sigma_{n-1} \leq \dots \leq \sigma_2 \leq \sigma_1 \quad (5.28)$$

We define the numerical rank r of X to be the number of singular values such that $\epsilon \leq \sigma_i$. Hence, the entries of X^+ can be expressed as

$$X_{ij}^+ = \sum_{k=1}^r \left(\frac{1}{\sigma_k} \right) v_{ik} \bar{u}_{jk} \quad (5.29)$$

By a theorem (i.e. [22]), the least-squares solution to a problem of the form given by Equation (5.25) is

$$\vec{N}_{1LS} = X^+ \vec{f} = V\Sigma^+U^* \vec{f} \quad (5.30)$$

If we assume that X is of full rank numerically, then there is a unique solution to Equation (5.25) given by

$$\vec{N}_1 = X^+ \vec{f} = V\Sigma^+U^* \vec{f} \quad r = n \quad (5.31)$$

Equation (5.30) is the scheme that has been coded to solve this problem. In cases where X is numerically of full rank, Equation (5.31) is actually implemented.

In solving for \vec{N}_1 , we obtain the values of the function $N_1(x)$ at n mesh points,

which means we are able to numerically solve the discretized version of Equation (3.27). We proceed to determine the scattered amplitudes by solving a discretized version of Equation (3.26). We shall use the same mesh for ξ and x as was used in solving for $N_1(x)$, and we have already set up the mechanics for the required numerical integration.

Recall that the integration on the left-hand side of Equation (3.27) for a given Bragg index was represented numerically by the left-hand side of Equation (4.28), with the row index i being related to the selected Bragg index by ν_i . We now construct the analogous representation for the integral expression in Equation (3.26), noting the relationship between ν and i given by Equation (5.11). We obtain

$$A_{(\nu_i)} = \left(\frac{1}{2\eta_i L} \right) \sum_{j=1}^n w_j K_{ij}^- N_{1j} \quad i = 1, 2, \dots, n \quad (5.32)$$

where

$$K_{ij}^- = e^{-ik_1(\eta_i s(x_j) + \xi_i x_j)} \quad (5.33)$$

and the values N_{1j} are now known. Equation (5.32) can be written in matrix-vector form as:

$$\vec{A} = Z \vec{N}_1 \quad (5.34)$$

where

$$Z_{ij} = \frac{w_j K_{ij}^-}{2\eta_i L} \quad (5.35)$$

Equations (4.32) - (4.37), (4.39) - (4.40), (5.11), and (5.24) all apply to Equations (5.33) - (5.35). It should be noted that the calculations for determining $A_{(\nu_i)}$, where i is such that $|\xi_i| \geq 1$, are not necessary since they apply to nonradiating surface waves. We only solve for $A_{(\nu_i)}$ associated with scattered waves (i.e. for i such that

$|\xi_i| < 1$).

Once the scattered amplitudes have been obtained, it is a simple matter to compute the summation given in Equation (3.31), relating to the conservation of energy. With the revised notation, this becomes

$$\sum_{i \text{ s.t. } |\xi_i| < 1} \left(\frac{\eta_i}{\beta} \right) |A_{(\nu_i)}|^2 = 1 \quad (5.36)$$

This relationship must hold if the calculated amplitudes are accurate.

It should also be mentioned that some flags and trouble-shooting mechanisms have been included in the code. The flag "info" is a subroutine output which reflects the reliability of the calculation of the singular values of the matrix X . The condition number of X and the residual $(\vec{f} - X\vec{N}_1)$ are also calculated to provide information regarding the stability of the system. In addition, in the event that very small singular values are present, the effective rank of the matrix is available. The finished driver code, which makes use of two LINPACK library subroutines, can be found in Appendix A.

Chapter 6

NUMERICAL RESULTS

In this chapter, our numerical scheme is applied to the classical problem of determining the amplitudes of the waves scattered from a sinusoidal surface. Consider the surface described by

$$z = s(x) = \left(-\frac{d}{2}\right) \left[1 + \cos\left(\frac{2\pi x}{L}\right)\right] \quad (6.1)$$

where, as shown in Figure (6.1), d represents the peak-to-trough depth and L describes the period. The highest surface excursion in the z -direction is $z = 0$, which occurs at $x = \frac{L}{2}(2n - 1)$, $n = 0, \pm 1, \pm 2, \dots$. An indication of surface roughness associated with

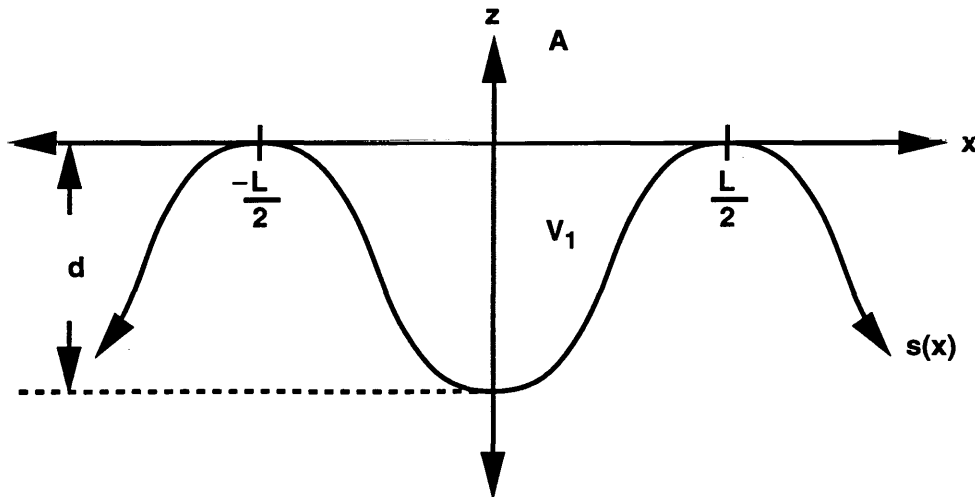


FIG. 6.1. Sinusoidal Surface

particular values of d and L can be given by the parameter $(\frac{d}{L})$, which we shall refer to as the “steepness” of the surface. Note that from the derivative of Equation (6.1), multiplying the steepness by π yields the maximum slope of the surface. Also, by selecting various values of d and L , one can produce an entire family of such sinusoidal surfaces.

A particular physical problem can be defined by the use of two surface characteristics, namely L and $(\frac{d}{L})$, where d and L are scaled to units of wavelength, and by one characteristic of the incident plane wave, namely θ_{inc} . Recall also that our solution scheme leaves us the option of varying the sample size n in our discretization, with the constraint that n must be large enough for the sample set to accommodate all scattered waves. We proceed to explore how changes in L , $(\frac{d}{L})$, θ_{inc} , and n may effect the accuracy of the numerical solution.

We begin the analysis with a discussion of varying the sample size n . Since L is to be expressed in units of wavelength, the sampling rate of the spatial variable x is $(\frac{n}{L})$ samples per wavelength. Hence, as n increases for a given L , the spatial mesh becomes finer. This would seem to enhance the accuracy of the numerical integrations performed. From Figure (5.2), one source of inaccuracy results from the fact that the staggered sample does not cover the entire domain $-\frac{L}{2} \leq x \leq \frac{L}{2}$. The numerical integration is actually performed over a domain which ignores a portion of the surface having length $\frac{L}{2(n-1)}$. Thus, as n is increased, the domain over which the numerical integration occurs approaches the true domain of x .

On the other hand, recall that given an α and an L , there is an integer approximately equal to $2L$, which represents the minimum allowable size of the sample set. This requirement serves to ensure that the set of ξ_i values selected includes all μ_ν that are associated with scattered waves. Recall also that it is legitimate to set n to

exceed that minimal requirement for the purpose of adding equations to the system which correspond to nonradiating surface waves. However, suppose that among the spectral samples there is an element ξ_i such that $|\xi_i| > 1$. Recall that from Equation (4.31), the entries in row i of matrix K^+ are given by

$$K_{ij}^+ = e^{ik_1(\eta_i s(x_j) - \xi_i x_j)} \quad j = 1, 2, \dots, n \quad (6.2)$$

and, since $|\xi_i| > 1$, Equation (4.33) stipulates that

$$\eta_i = +i\sqrt{\xi_i^2 - 1} \quad (6.3)$$

Therefore, the moduli of such entries are

$$|K_{ij}| = e^{-k_1 s(x_j) \sqrt{\xi_i^2 - 1}} \quad j = 1, 2, \dots, n \quad (6.4)$$

So, consider the process of adding two new samples to a sample set. From the discussion following Equation (5.10), one new sample is added to each side of the distribution, and thus, Equation (4.32) implies that the absolute value of the new ξ_1 is larger than that of the old ξ_1 , (which is now ξ_2). Similarly, the absolute value of the new ξ_n is larger than that of the old ξ_n (which is now ξ_{n-1}). Also, since the $s(x)$ values of the surface defined in Equation (6.1) are all non-positive, Equation (6.4) implies that the magnitudes of the entries in rows 1 and n are larger than the magnitudes of the entries in rows 2 and $(n - 1)$, respectively. Such changes in magnitude from row to row are exponential so that in a matrix which accommodates many nonradiating surface waves, the moduli of the entries in the outer rows may be several orders of magnitude larger than moduli of those in the middle rows (which, by Equations (4.31)

- (4.33), are equal to one). The condition numbers of such matrices are typically quite large.

It should also be mentioned that if we were to translate $s(x)$ vertically by $\Delta z = +d$, then all the values of $s(x)$ would be non-negative. In this case, if the matrix K^+ housed many rows corresponding to nonradiating surface waves, the moduli of the entries in the outer rows would this time be dominated by the moduli of the entries in the middle rows (which equal one), again causing K^+ to be ill-conditioned. A study to be considered for future work would be to examine a possible optimal z -orientation of the surface so as to minimize the condition number of K^+ . Such translations do not affect the resulting scattered intensities. In addition, it should be mentioned that the application of certain discretization weights could have an impact on the preceding discussion. However, in this particular study, it seemed that when K^+ was ill-conditioned, so was X .

To summarize the discussion so far, an increase in n should improve the accuracy of the numerical integrations due to implementing a finer mesh. However, an increase in n serves to add rows whose entries are larger in magnitude than the entries in the existing rows. Since this growth from row to row is exponential, the moduli of the entries in the outer rows may be several orders of magnitude larger than the moduli of the entries in the middle rows. Thus, without the use of row scaling (which will be discussed later), the condition number of the matrix increases. So there are advantages and disadvantages associated with adding equations to the system which correspond to nonradiating surface waves. Thus, the objective is to learn more about the nature of the tradeoffs involved so that for any particular problem, n can be chosen so as to attain the highest level of accuracy available.

We proceed by considering a concrete example, where

$$L \sim 20\lambda_1 \quad (6.5)$$

and

$$\theta_{inc} = 0^\circ \quad (6.6)$$

In order to explain the notation used in Equation (6.5), some background is required. The term “grazing”, as used to describe an incident or scattered wave, refers to a wave propagating in a direction nearly parallel to the x -axis (nearly perpendicular to the z -axis). Waves which scatter at grazing angles are associated with Bragg indices such that $|\mu_\nu| \approx 1$ and $|\mu_\nu| < 1$. For our particular example, we shall choose $L = 20.0005$ (wavelengths) so that the scattered angles associated with Bragg indices $\nu = \pm 20$ are $\theta_{sc} = \pm 89.6^\circ$. Had we chosen $L = 20$, the outermost scattered angles would have been $\theta_{sc} = \pm 71.8^\circ$, associated with Bragg indices $\nu = \pm 19$. These values for θ_{sc} come from Equations (3.28) and (3.30). If one uses $L = 20$ and $\nu = \pm 20$, the associated “scattered” angles are $\theta_{sc} = \pm 90^\circ$, and since waves “scattered” horizontally cannot reach region A in Figure (1.1), then they are not part of the scattered spectrum in region A .

Hence, by decreasing L from 20.0005 to 20, the number of scattered waves decreases from 41 to 39, and the outermost scattered angles occur at $\theta_{sc} = \pm 71.8^\circ$ rather than at $\theta_{sc} = \pm 89.6^\circ$. If we were to take $L = 20.0005$, and shift the angle of incidence from $\theta_{inc} = 0^\circ$ to $\theta_{inc} = 5^\circ$, we would only have 40 scattered waves, but by taking $L = 20.25$ and $\theta_{inc} = 5^\circ$, we would obtain 41 again. The point is that for the purpose of including data for scattered angles near grazing, we use a general guideline for L , and determine the appropriate exact L to accommodate the given θ_{inc} . This

also serves to provide a basis for consistency when studying the effects of varying θ_{inc} for a given (approximate) value of L . This explains the notation given in Equation (6.5).

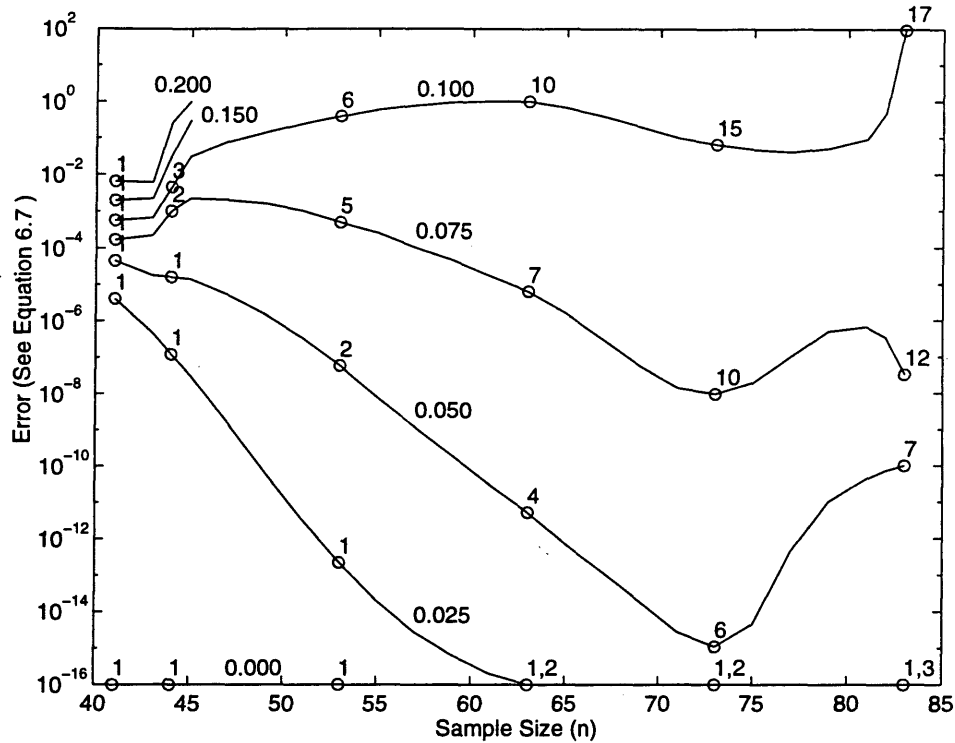
So, for $\theta_{inc} = 0^\circ$ and $L \sim 20$ (actual L is 20.0005 in this case), the code in Appendix A was used to generate results for various sample sizes ranging from $n = 41$ to $n = 83$. For such L and θ_{inc} , $n = 41$ is associated with a sample set corresponding to exactly the set of scattered waves, and a spatial sampling rate of 2.05 samples per wavelength. The sample set of size $n = 83$ includes the 41 scattered spectral values as well as 42 nonradiating spectral values. The associated spatial sampling rate is 4.15 samples per wavelength.

One measurement of the accuracy of the solution is given by

$$Error \equiv \left| 1 - \sum_{i \text{ s.t. } |\xi_i| < 1} \left(\frac{\eta_i}{\beta} \right) |A(\nu_i)|^2 \right| \quad (6.7)$$

which comes from the energy-conservation relationship of Equation (5.36). The results for different values of $(\frac{d}{L})$ are plotted in Figure (6.2). Figure (6.2) reveals much information about the nature of the tradeoffs involved with the inclusion of nonradiating surface waves in the sample. We begin with the obvious observation that the accuracy of the results worsens as the steepness $(\frac{d}{L})$ is increased (i.e. as the surface becomes rougher), and this behavior holds regardless of the sample size. Note that $(\frac{d}{L}) = 0$ is the case of a perfectly flat surface $z = s(x) \equiv 0$.

As is pointed out in the figure's legend, the small numbers next to the data points represent $\log_{10}[cond(X)]$, where $cond(X)$ denotes the condition number of X . These numbers provide information regarding for the order of magnitude of the condition number of X in each program run. As expected, and as discussed in the text following Equation (6.4), the condition number of X increases as n increases.



Legend

Each curve is associated with a value of (d/L) , as labelled

Each data point on the curve is associated with a condition number of X . The points are labelled with $\log_{10}[\text{cond}(X)]$.

The domain of n is discrete, and the curves have been added to indicate trends.

FIG. 6.2. Error vs n , $L \sim 20\lambda_1$, $\theta_{inc} = 0^\circ$

Figure (6.2) clearly demonstrates that this trend holds for all values of $(\frac{d}{L})$.

We now consider the results obtained using $n = 41$, which is the sample set consisting solely of scattered waves. For such n , the accuracy, in terms of energy conservation, is better than 99% for values of $(\frac{d}{L})$ up to and including $(\frac{d}{L}) = 0.200$.

Also note that the condition number of X for all such $(\frac{d}{L})$ is on the order of 10^1 (i.e. $O(10^1)$), for $n = 41$. The behavior of the curves in Figure (6.2) illustrate when it is advantageous to add some nonradiating spectral samples, and when such a strategy is detrimental.

For the flat surface case (i.e. $(\frac{d}{L}) = 0$), *Error* (see Equation (6.7)) attains machine accuracy, regardless of n . However, it is clear that there exist sample sizes n such that machine accuracy is attained for $(\frac{d}{L}) = 0.025$, whereas for $n = 41$, the error is $O(10^{-6})$. It is also clear that increasing n is advantageous for $(\frac{d}{L}) = 0.050$ and for $(\frac{d}{L}) = 0.075$, with the optimal sample size in both cases being $n = 73$ (i.e. 32 nonradiating spectral samples, 3.65 spatial samples per wavelength).

On the other hand, it is obvious from the graph that for $(\frac{d}{L}) \geq 0.100$, it is better to keep $n = 41$, or to add exactly two spectral samples to the set. For such $(\frac{d}{L})$, once n reaches 45 and higher, *Error*, as defined in Equation (6.7), exceeds 1%. In some cases it jumps to 2%, which may still be acceptable in practice, but in other cases, the jumps are far greater.

It is important to understand the behavior of the curves in Figure (6.2) because this general behavior was evident for a variety of values of L and θ_{inc} , and the “cut-off value” for $(\frac{d}{L})$ was always observed to be between 0.075 and 0.100 for $L \sim 20$, regardless of θ_{inc} .

One additional trend worth mentioning is the rate at which $cond(X)$ increases as a function of n . Notice that this increase is considerably faster for larger values of $(\frac{d}{L})$. This behavior is the direct result of Equation (6.4). For small values of $(\frac{d}{L})$, $|s(x)|$ remains fairly small, whereas for large values of $(\frac{d}{L})$, large values of $|s(x)|$ can occur. Thus, the phenomenon of growth of the moduli of the entries in the outer rows of X is further amplified by large negative $s(x)$ values.

With all of the preceding discussion in mind, we proceed to examine the curves in Figure (6.2) corresponding to $(\frac{d}{L}) = 0.075$ and $(\frac{d}{L}) = 0.100$. This will be instructive since the cutoff point for the applicability of the two strategies (i.e. either consider spectral samples relating to surface waves or do not) lies between those values.

Recall that the argument for increasing n is the improved accuracy of the numerical integrations due to a finer spatial mesh, and the argument against increasing n is the subsequent increase in the condition number of the matrix X . Note that for the $(\frac{d}{L}) = 0.075$ curve, the former argument dominates the latter one. To explain why, we must first discuss the concept of an ill-conditioned system.

When a matrix operates on a vector containing erroneous data, those errors become incorporated into the solution. If that matrix is ill-conditioned (i.e. its condition number is large), the solution may inherit a greatly-magnified version of those errors. In effect, a large condition number relaxes the bound for error in the solution so that the potential for amplified error in the solution exists. Whether or not that potential is realized for a given problem depends upon the actual vector being operated on.

Although the condition number for X in the $(\frac{d}{L}) = 0.075$ case is quite large for large n , the overall accuracy (in terms of energy conservation) of the results is quite good. Thus, it seems that either the errors in the system are on the order of machine accuracy (so that even when magnified, they are negligible), or the actual error is not approaching the relaxed bounds resulting from the ill-conditioning. Indeed, both factors may contribute to keeping the error in the solution small.

We turn our attention now to the $n = 45$ point on the $(\frac{d}{L}) = 0.100$ curve. Its condition number is nine orders of magnitude smaller than that of the $n = 83$ point on the $(\frac{d}{L}) = 0.075$ curve, yet the overall accuracy is considerably worse. It seems that

the error must lie in the spatial discretization here. Logically, as $s(x)$ becomes rougher (i.e. as $(\frac{d}{L})$ increases), a somewhat small spatial sample is insufficient to accurately represent its rapidly-changing behavior. This large inaccuracy is at a “manageable” level for $n = 41$ and $n = 43$ because the condition number is only $O(10^1)$. However, by $n = 45$, the condition number is $O(10^3)$, and the large inaccuracies are magnified beyond recovery.

As we move further to the right along the $(\frac{d}{L}) = 0.100$ curve, we expect the increase in the number of spatial samples per wavelength to decrease the error in the system. However, although this is the case, the condition number is so large by the time this occurs that even the resulting small errors in the data are magnified to the point where they are significant in the solution.

Finally, we make some remarks about the apparent optimal sampling size of $n = 73$. It seems that for $(\frac{d}{L}) = 0.050$ and $(\frac{d}{L}) = 0.075$, $n = 73$ is the point at which the advantages resulting from making the mesh finer are finally outweighed by the growing condition number.

Now that Figure (6.2) has been thoroughly analyzed, it should be clear that for a given problem, it is possible to construct a similar graph empirically, from which it is possible to determine the optimal sample size to use. For the remainder of this paper, we shall assume that this procedure is implemented and that all results given from here on correspond to that optimal n .

As was stated earlier, *Error*, as defined by Equation (6.7), increases as $(\frac{d}{L})$ is increased for a given L and θ_{inc} . This relationship is shown in a more detailed form in Figure (6.3) for various values of θ_{inc} . We continue to hold $L \sim 20$, although as θ_{inc} progresses from normal incidence to grazing incidence, the exact value of L is varied so as to retain 41 scattered waves and to keep the outer scattered angles as close to

$\pm 90^\circ$ as possible. Table (6.1) displays such details for three distinct incident angles.

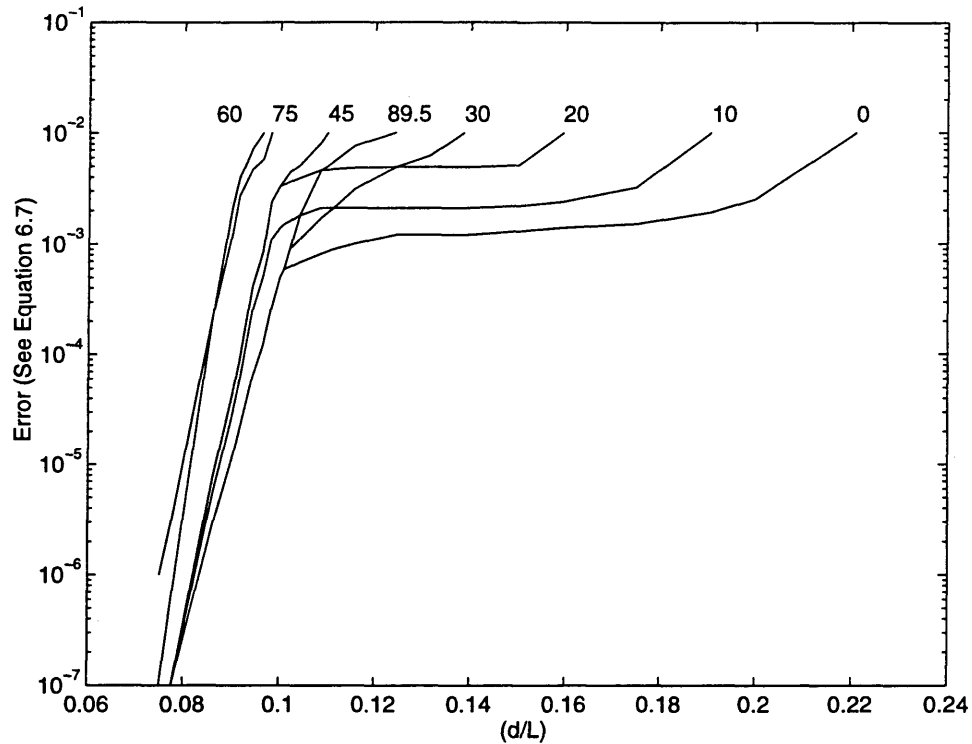


FIG. 6.3. Error vs $(\frac{d}{L})$, where $L \sim 20\lambda_1$, for selected values of θ_{inc}

From Figure (6.2), it is clear that for $(\frac{d}{L}) \leq 0.050$, we can nearly attain machine accuracy (in terms of energy conservation), so we focus our analysis on larger $(\frac{d}{L})$ values in Figure (6.3). Also, we choose to study only the regions in which 99% accuracy (i.e. $Error \sim 10^{-2}$) or better is attained. Notice the “knee-shaped” nature of the curves in Figure (6.3), which is evident for all incident angles shown. The knee is very sharp for small values of θ_{inc} and it becomes less severe until $\theta_{inc} = 60^\circ$, then it becomes slightly sharper again. This behavior is indicative of the fact that 99%

Table 6.1. Bragg Indices and Scattered Angles, $L \sim 20\lambda_1$

Row Index (i)	$\theta_{inc} = 0^\circ, L = 20.0005$ $\frac{\text{Samples}}{\text{Wavelength}} = 4.15$		$\theta_{inc} = 20^\circ, L = 20.1250$ $\frac{\text{Samples}}{\text{Wavelength}} = 4.12$		$\theta_{inc} = 60^\circ, L = 20.4000$ $\frac{\text{Samples}}{\text{Wavelength}} = 4.07$	
	Bragg Index (ν_i)	Scattered Angle (θ_{sc})	Bragg Index (ν_i)	Scattered Angle (θ_{sc})	Bragg Index (ν_i)	Scattered Angle (θ_{sc})
1	-20	-89.6°	-27	-88.4°	-38	-85.4°
2	-19	-71.8°	-26	-71.8°	-37	-71.4°
3	-18	-64.2°	-25	-64.2°	-36	-64.0°
4	-17	-58.2°	-24	-58.3°	-35	-58.2°
5	-16	-53.1°	-23	-53.2°	-34	-53.2°
6	-15	-48.6°	-22	-48.7°	-33	-48.7°
7	-14	-44.4°	-21	-44.5°	-32	-44.6°
8	-13	-40.5°	-20	-40.7°	-31	-40.8°
9	-12	-36.9°	-19	-37.0°	-30	-37.2°
10	-11	-33.4°	-18	-33.5°	-29	-33.7°
11	-10	-30.0°	-17	-30.2°	-28	-30.4°
12	-9	-26.7°	-16	-26.9°	-27	-27.2°
13	-8	-23.6°	-15	-23.8°	-26	-24.1°
14	-7	-20.5°	-14	-20.7°	-25	-21.1°
15	-6	-17.5°	-13	-17.7°	-24	-18.1°
16	-5	-14.5°	-12	-14.7°	-23	-15.2°
17	-4	-11.5°	-11	-11.8°	-22	-12.3°
18	-3	-8.6°	-10	-8.9°	-21	-9.4°
19	-2	-5.7°	-9	-6.0°	-20	-6.6°
20	-1	-2.9°	-8	-3.2°	-19	-3.7°
21	0	0.0°	-7	-0.3°	-18	-0.9°
22	1	2.9°	-6	2.5°	-17	1.9°
23	2	5.7°	-5	5.4°	-16	4.7°
24	3	8.6°	-4	8.2°	-15	7.5°
25	4	11.5°	-3	11.1°	-14	10.4°
26	5	14.5°	-2	14.0°	-13	13.2°
27	6	17.5°	-1	17.0°	-12	16.1°
28	7	20.5°	0	20.0°	-11	19.1°
29	8	23.6°	1	23.1°	-10	22.1°
30	9	26.7°	2	26.2°	-9	25.1°
31	10	30.0°	3	29.4°	-8	28.3°
32	11	33.4°	4	32.7°	-7	31.5°
33	12	36.9°	5	36.2°	-6	34.9°
34	13	40.5°	6	39.8°	-5	38.4°
35	14	44.4°	7	43.6°	-4	42.1°
36	15	48.6°	8	47.7°	-3	46.0°
37	16	53.1°	9	52.1°	-2	50.2°
38	17	58.2°	10	57.0°	-1	54.8°
39	18	64.2°	11	62.7°	0	60.0°
40	19	71.8°	12	69.8°	1	66.2°
41	20	89.6°	13	81.1°	2	74.6°

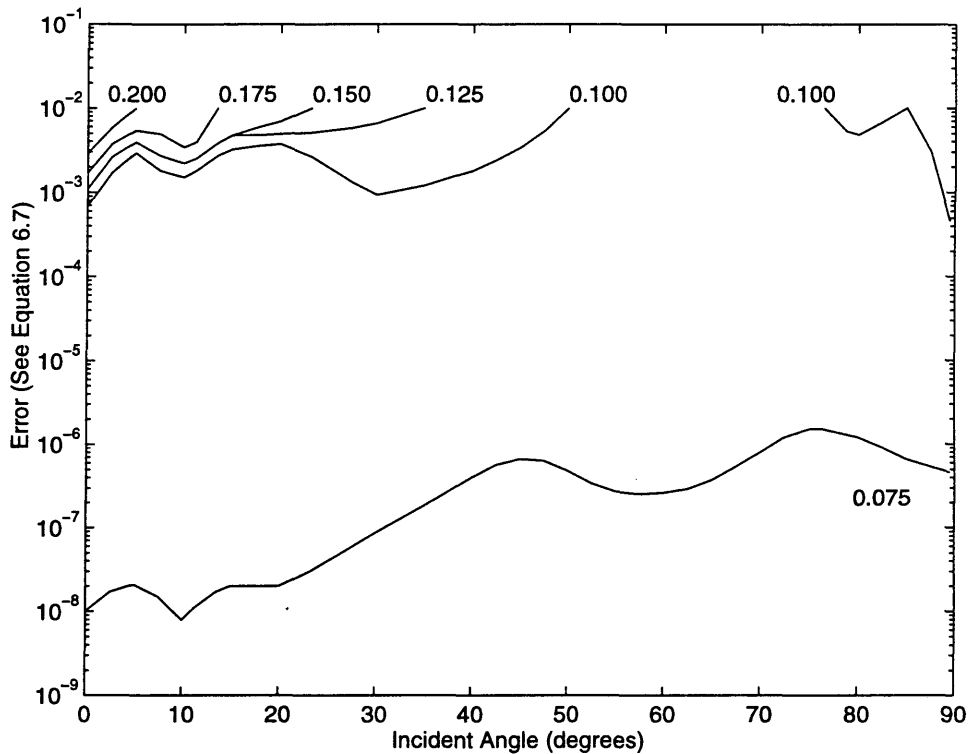


FIG. 6.4. Error vs θ_{inc} , where $L \sim 20\lambda_1$, for selected values of $(\frac{d}{L})$

accuracy is attainable for much larger $(\frac{d}{L})$ values in the case of normal incidence than in the case of 60° incidence, for example. In fact, the results are more accurate for near-grazing incidence than they are in the $\theta_{inc} = 60^\circ$ to $\theta_{inc} = 75^\circ$ range. Figure (6.4) displays these same results from a different perspective. It should be noted that the range from $\theta_{inc} = 60^\circ$ to $\theta_{inc} = 75^\circ$ consistently provided the least accurate results as $(\frac{d}{L})$ and L were varied.

So far we have explored the manner in which variations in θ_{inc} , $(\frac{d}{L})$, and n affect the overall accuracy of the results, but we have worked with $L \sim 20\lambda_1$ in all cases. It is appropriate then, to make some remarks about the influence of L on the level

of accuracy. Figure (6.5) provides information concerning normal incidence for three distinct surfaces, each having a different associated L value. From the figure, it is apparent that for values of $(\frac{d}{L})$ ranging from 0.075 to 0.125, higher levels of accuracy (in terms of energy conservation) are attainable for smaller values of L . On the other hand, when $(\frac{d}{L})$ is larger (i.e. ranging from 0.150 to 0.200), the higher levels of accuracy are associated with the larger values of L .

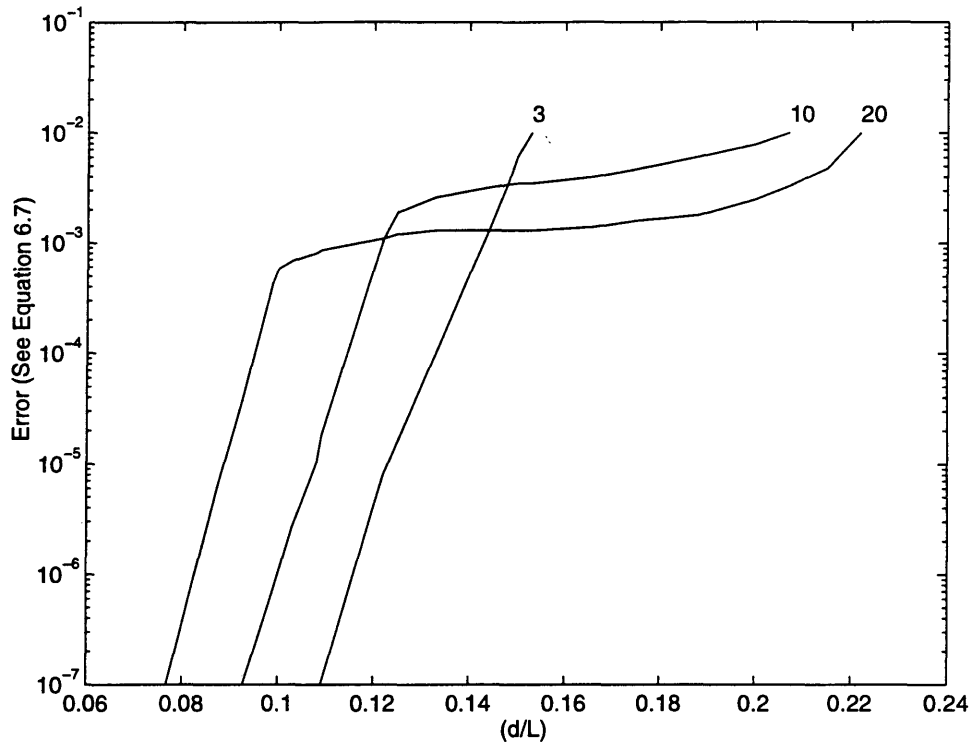


FIG. 6.5. Error vs $(\frac{d}{L})$, where $\theta_{inc} = 0^\circ$, for $L = 3, 10,$ and 20

The reason that $L \sim 3$ can attain such a high level of accuracy for relatively small values of $(\frac{d}{L})$ (i.e. for $(\frac{d}{L}) \leq 0.100$) lies in the fact that very fine spatial meshes can

be represented using relatively small matrices. For example, a 41-by-41 system for $L \sim 3\lambda_1$ is associated with a spatial sampling rate of 13.67 samples per wavelength, whereas a 41-by-41 system for $L \sim 20\lambda_1$ is associated with only 2.0 samples per wavelength.

However, for $n = 41$ and $L \sim 3$, there are only 7 rows in the system matrix corresponding to scattered waves, and 34 corresponding to nonradiating surface waves. Thus, following the discussion earlier in this chapter regarding Figure (6.2), we expect the condition number of such a matrix to be fairly large. On the other hand, for $n = 41$ and $L \sim 20$, every row corresponds to a scattered wave so that the condition number is quite small. Thus, for smaller values of $(\frac{d}{L})$, the high condition number seems to play a reduced role in the $L \sim 3$ case since the mesh is extremely fine, and errors in the system are therefore minimal. Thus, for such $(\frac{d}{L})$, the $L \sim 3$ errors are significantly smaller than the $L \sim 20$ errors. Note that a coarser mesh was utilized for $L \sim 20$.

However, as $(\frac{d}{L})$ becomes larger, the condition number for $L \sim 3$ becomes so large that even the seemingly insignificant errors provided by the ultrafine mesh are magnified to the point where the overall error in the solution is quite significant. Thus, for such $(\frac{d}{L})$, the well-conditioned system for $L \sim 20$, $n = 41$, and approximately 2 samples per wavelength attains better results than the ill-conditioned system for $L \sim 3$, $n = 41$, and approximately 14 samples per wavelength.

This completes the analysis of the numerical errors involved in this approach. We conclude this chapter with a few remarks regarding the 1992 article of Bishop and Smith [8]. In particular, the article states that “the DeSanto theory became numerically unstable for $(\frac{a}{\Lambda}) \sim 0.05$.” In Bishop’s notation, Λ represents the period of the surface and “ a ” represents the amplitude of the surface. Thus, Bishop’s Λ is

analogous to our L , and Bishop's "a" is analogous to our $(\frac{d}{2})$. So Bishop essentially claims that the DeSanto theory became numerically unstable for $(\frac{d}{L}) \sim 0.100$.

We point out here that Bishop's system of equations is not a discretization of Equations (4.29) - (4.40), but rather is a system that was derived using a physical optics representation of the surface field, which yielded Bessel functions as the matrix coefficients. Bishop's equations are akin to those found in DeSanto's paper [5]. The purpose of this particular discussion is to demonstrate that using the system of equations developed in this paper, we can obtain high levels of accuracy, in terms of energy conservation, where Bishop's technique ran into difficulties.

Bishop's parameters were $k = 50 \text{ m}^{-1}$, $\theta_g = 90^\circ$, $\Lambda = 2.0 \text{ m}$, and $(\frac{a}{\Lambda}) = 0.05$. We begin by converting his parameters to our notation. We have from Equation (1.6),

$$k_1 = 50 = \frac{2\pi}{\lambda_1} \quad (6.8)$$

so that

$$\lambda_1 = 0.1257 \text{ m} \quad (6.9)$$

Also,

$$\frac{d}{L} = \frac{2a}{\Lambda} = 0.100 \quad (6.10)$$

We convert all measurements to units of wavelength so that

$$L = \Lambda = \frac{2.0 \text{ m}}{0.1257 \frac{\text{m}}{\lambda_1}} = 15.9\lambda_1 \quad (6.11)$$

Combining Equations (6.10) and (6.11) yields

$$d = 1.59\lambda_1 \quad (6.12)$$

Also, $\theta_g = 90^\circ$ in Bishop's notation corresponds to

$$\theta_{inc} = 0^\circ \tag{6.13}$$

in our notation. Thus, we use the information in Equations (6.11), (6.12), and (6.13) from our code (in Appendix A), and examine the results. There are exactly 31 physical scattered waves associated with this problem, and it turns out that in this case, the minimal value of *Error*, as defined in Equation (6.7), is associated with $n = 73$. The results are provided in Table (6.2).

From Table (6.2), it seems likely that this is an accurate result since energy is conserved to within 0.001%. Note that the table also indicates that our matrix, like Bishop's, has a high condition number. However, these results further support the argument earlier in this chapter that ill-conditioned systems can still produce highly accurate solutions, in terms of energy conservation. In addition, small residuals were observed in such cases.

Table (6.3) indicates that we can obtain results of approximately 99% energy-conservation accuracy with nearly twice the $(\frac{d}{L})$ ratio at which Bishop's system ran into difficulties. Table (6.4) illustrates that for the surface at which Bishop experienced problems for normal incidence, our code provides 0.025% energy-conservation accuracy for near-grazing incidence.

Table 6.2. Results for $L = 15.9\lambda_1$, $(\frac{d}{L}) = 0.100$, and $\theta_{inc} = 0^\circ$

Length (wavelengths) :		15.9000		
d/L		0.100		
Incident Angle (degrees) :		0.0		
Total Number of Samples :		73		
Samples per Wavelength :		4.59		
# of Physical Scattered Angles :		31		
Effective Rank Used :		73		
Bragg Index	Scattered Angle	Scattered Amplitudes Magnitude	real	imaginary
-15	-70.6	0.003244	-0.000669	0.003174
-14	-61.7	0.001205	-0.000718	-0.000967
-13	-54.8	0.004264	0.004248	0.000376
-12	-49.0	0.017633	0.004397	-0.017076
-11	-43.8	0.062892	-0.045836	-0.043063
-10	-39.0	0.145332	-0.124371	0.075187
-9	-34.5	0.274952	0.084781	0.261554
-8	-30.2	0.366528	0.364111	-0.042029
-7	-26.1	0.324312	0.016629	-0.323885
-6	-22.2	0.079255	-0.077130	-0.018230
-5	-18.3	0.209768	0.065396	-0.199314
-4	-14.6	0.251174	-0.230806	-0.099083
-3	-10.9	0.031157	0.014855	-0.027387
-2	-7.2	0.257398	-0.222405	-0.129576
-1	-3.6	0.049873	-0.026435	0.042291
0	0.0	0.244739	-0.206961	-0.130631
1	3.6	0.050644	-0.025662	0.043661
2	7.2	0.257951	-0.223174	-0.129352
3	10.9	0.032772	0.016808	-0.028134
4	14.6	0.251568	-0.230886	-0.099888
5	18.3	0.210240	0.064587	-0.200074
6	22.2	0.078868	-0.077317	-0.015563
7	26.1	0.321793	0.017422	-0.321321
8	30.2	0.368474	0.366084	-0.041893
9	34.5	0.272483	0.085075	0.258861
10	39.0	0.146631	-0.125402	0.075993
11	43.8	0.063624	-0.047260	-0.042597
12	49.0	0.017092	0.008366	-0.014904
13	54.8	0.002484	0.001270	-0.002135
14	61.7	0.001409	-0.000238	0.001389
15	70.6	0.001401	-0.001308	0.000502
Normalized Energy :		1.00000954234783		
Condition Number :		0.1978E+16		

Table 6.3. Results for $L = 15.9\lambda_1$, $(\frac{d}{L}) = 0.195$, and $\theta_{inc} = 0^\circ$

Length (wavelengths) :	15.9000			
d/L	0.195			
Incident Angle (degrees) :	0.0			
Total Number of Samples :	33			
Samples per Wavelength :	2.08			
# of Physical Scattered Angles :	31			
Effective Rank Used :	33			
Bragg Index	Scattered Angle	Scattered Amplitudes Magnitude	real	imaginary
-15	-70.6	0.217998	-0.114114	0.185745
-14	-61.7	0.409618	-0.072004	0.403240
-13	-54.8	0.496512	0.161739	0.469430
-12	-49.0	0.131833	0.124174	0.044282
-11	-43.8	0.226025	-0.194177	0.115682
-10	-39.0	0.229613	-0.011573	0.229321
-9	-34.5	0.114486	-0.100942	-0.054016
-8	-30.2	0.208681	-0.162719	0.130653
-7	-26.1	0.025683	-0.004242	-0.025330
-6	-22.2	0.212549	-0.211128	0.024533
-5	-18.3	0.006244	-0.004858	-0.003923
-4	-14.6	0.187192	-0.176406	-0.062626
-3	-10.9	0.023750	-0.007723	0.022459
-2	-7.2	0.181395	-0.155254	-0.093811
-1	-3.6	0.031808	-0.018963	0.025538
0	0.0	0.177522	-0.142881	-0.105352
1	3.6	0.029504	-0.016951	0.024148
2	7.2	0.183988	-0.156402	-0.096902
3	10.9	0.027113	-0.012947	0.023823
4	14.6	0.183908	-0.175499	-0.054975
5	18.3	0.006694	0.005251	-0.004152
6	22.2	0.210811	-0.210432	0.012637
7	26.1	0.032267	-0.016653	-0.027638
8	30.2	0.221150	-0.168562	0.143158
9	34.5	0.094975	-0.084874	-0.042621
10	39.0	0.201026	0.001656	0.201019
11	43.8	0.267838	-0.240444	0.118000
12	49.0	0.191036	0.168145	0.090676
13	54.8	0.416136	0.155665	0.385925
14	61.7	0.510789	-0.115899	0.497467
15	70.6	0.096249	-0.033213	0.090337
Normalized Energy :	1.01042215197199			
Condition Number :	0.5195E+02			

Table 6.4. Results for $L = 15.9\lambda_1$, $(\frac{d}{L}) = 0.100$, and $\theta_{inc} = 89.5^\circ$

Length (wavelengths) :		15.9000		
d/L		0.100		
Incident Angle (degrees) :		89.5		
Total Number of Samples :		71		
Samples per Wavelength :		4.47		
# of Physical Scattered Angles :		32		
Effective Rank Used :		71		
Bragg Index	Scattered Angle	Scattered Amplitudes Magnitude	real	imaginary
-31	-71.8	0.000028	0.000016	0.000023
-30	-62.5	0.000019	-0.000016	0.000010
-29	-55.5	0.000014	-0.000004	-0.000014
-28	-49.6	0.000014	0.000014	-0.000001
-27	-44.3	0.000008	-0.000002	0.000008
-26	-39.4	0.000007	-0.000006	-0.000003
-25	-34.9	0.000003	0.000001	-0.000003
-24	-30.6	0.000001	0.000001	0.000001
-23	-26.5	0.000002	-0.000001	0.000001
-22	-22.6	0.000001	-0.000001	0.000000
-21	-18.7	0.000002	-0.000001	0.000002
-20	-14.9	0.000003	0.000002	-0.000002
-19	-11.2	0.000000	0.000000	0.000000
-18	-7.6	0.000001	-0.000001	0.000000
-17	-4.0	0.000001	-0.000001	-0.000001
-16	-0.4	0.000004	0.000002	0.000003
-15	3.2	0.000001	-0.000001	0.000001
-14	6.9	0.000003	0.000002	0.000001
-13	10.5	0.000003	-0.000002	-0.000002
-12	14.2	0.000009	-0.000004	0.000008
-11	17.9	0.000029	0.000027	0.000011
-10	21.8	0.000093	0.000025	-0.000089
-9	25.7	0.000259	-0.000257	-0.000035
-8	29.8	0.000645	0.000022	0.000644
-7	34.0	0.001447	0.001405	-0.000345
-6	38.5	0.002911	-0.001369	-0.002568
-5	43.3	0.005214	-0.003652	0.003721
-4	48.5	0.008299	0.007642	0.003236
-3	54.2	0.011700	-0.000888	-0.011667
-2	60.9	0.014899	-0.011296	0.009714
-1	69.6	0.019466	0.019455	-0.000669
0	89.5	0.977013	-0.976093	-0.042402
Normalized Energy :		0.99975034435139		
Condition Number :		0.7067E+15		

Chapter 7

CONCLUSIONS

In this thesis, we have considered a physical setting in which a perfectly-reflecting periodic surface is subjected to an incident plane wave, under the assumption that the total field is equal to zero everywhere on the surface. DeSanto's work [6] states that in such a scenario, the scattered field above the highest surface excursion consists of a discrete spectrum of upgoing plane waves, and his "Spectral-Coordinate" formalism provides an expression for the scattered amplitudes involving the solution of a first-kind integral equation.

This thesis has served to design and develop a FORTRAN code to be utilized in a numerical solution of the problem. The accuracy of the solutions generated here is gauged by the degree to which the physical requirement of energy conservation is fulfilled. Upon applying the code to the classical sinusoidal surface problem, we have seen that the solutions are of machine precision for relatively smooth surfaces, and that 99% accuracy, in terms of energy conservation, is attainable for somewhat rougher surfaces.

A particularly interesting feature of this code is the high level of accuracy, in terms of energy conservation, attained for near-grazing angles of incidence. Although grazing incidence has historically caused numerical difficulties, solutions of machine precision are available when applying our code to sufficiently-smooth surfaces. It should be mentioned that the past numerical solutions, to the best of the author's knowledge, did not make use of the particular equations utilized in this paper. Bishop, for example, has generated results by numerically solving a set of equations which

follows from DeSanto's theory and a physical optics expansion of the surface field to yield Bessel functions [8]. His system becomes "ill-conditioned" (although the term is not defined quantitatively in his paper [8]) for normal incidence and a certain degree of roughness, whereas our results for that same surface attain an energy-conservation accuracy level of approximately 0.025% for near-grazing incidence.

Another particular strength of our code lies in the fact that it has been designed to accommodate periodic surfaces that are of arbitrary geometry within the period. One possible area of future work could involve studying the performance of this code when applied to a wide variety of surface functions, or indeed to cases where the surface geometry is described only by a set of data points, which may have been obtained by empirical measurements.

Although the energy check seems to have historically been the primary tool for assessing the accuracy for numerical results for scattering problems, it is important to realize that the fulfillment of the energy conservation requirement is a necessary, but not a sufficient, criterion for the solution to meet. Unfortunately, due to the complexity of the equations involved, there are very few physical problems for which the exact solution is known (such problems could serve as a basis for judging the accuracy of solutions generated by a given numerical technique). However, certain steps have been taken toward assessing the accuracy of the solutions produced by the code developed in this paper.

One procedure in which errors are introduced is the process of solving the linear system for the discretized version of the function $N_1(x)$. The magnitude of the error in the energy check for a given program execution seemed to be related to the norm of the residual in the solution of the linear system, with the highest levels of accuracy in energy conservation corresponding to the lowest values of the residual norm. In

addition, in cases where the energy check was highly accurate, the associated values of the solution vector \vec{N}_1 were of a magnitude consistent with their physical meaning. Also, for some physical problems, increasing the sample size served to increase the condition number of the matrix by several orders of magnitude, yet the accuracy of the energy check improved due to a finer spatial mesh. In such instances, there was minimal difference in the final solutions (in the scattered amplitudes) obtained by using the well-conditioned system (having a smaller sample size) and by using the ill-conditioned system (having a larger sample size). This tends to indicate that the final solutions generated are accurate, yet of course, this is not proof.

The exact solution is known for the trivial flat-surface case, and our code matched that solution to machine accuracy. Perhaps piecewise-linear surface functions would be analytically solvable, thereby serving as test surfaces for future studies of the accuracy of final solutions.

As was mentioned earlier, the error in numerical integration using the “generalized” Simpson’s Rule [16], is on the order of the cube of the largest spatial interval length. Such error could be reduced by interpolating with a polynomial of higher order. We have also seen the effects of increasing the number of spectral samples in the system (by adding equations associated with nonradiating surface waves). The order of error involved in truncating Equation (4.19) to obtain Equation (4.28) is difficult to obtain. Equation (4.28) could be posed for infinitely many values of n , and the set of solutions associated with those values could be arranged in the form of a sequence. If the sequence converged to the solution given by Equation (4.19), then the knowledge of the rate of that convergence could be used to evaluate the error associated with spectral truncation.

One general result obtained empirically in this paper is that the addition of

equations relating to surface waves serves to increase the condition number of the matrix. Hence, one approach worth studying would be that which utilizes a non-square system, so as to receive the benefits of having a large spatial sample set (and hence a fine mesh for numerical integration), while attempting to somewhat dampen the growth of system instability by keeping the number of spectral samples to a minimum.

Another consideration for the future could be the use of a Lagrange multiplier technique [23], in which the normalized energy is constrained to equal one. This would guarantee the fulfillment of the energy conservation requirement. Also, the accuracy of the numerical integrations may be improved through equidistribution [24] of the spatial mesh. The principle is to evenly distribute the local error so as to sample the spatial variable more frequently in areas where the integrand varies more rapidly.

There are also schemes available for attempting to reduce high condition numbers. One such technique is equilibration, or row scaling [25]. This procedure can often be used to counter the effect of adding rows (associated with surface waves in this problem) which have much larger entries in magnitude than the existing rows. Unfortunately, even matrices which have been row-scaled could remain ill-conditioned.

A second method of attempting to improve stability is that of regularization [26], in which errors in the system's data are dampened somewhat. One common technique for accomplishing this is Least-Squares Minimization with Quadratic Inequality Constraint (LSQI) [27]. Yet another way of trying to deal with the ill-conditioned systems is to truncate "troublesome" singular values. This option is available with the pseudo-inverse approach [22], although we have yet to exercise it.

It should finally be mentioned that the theory for dealing with variations on the problem studied here has been developed. For example, one could consider alternative

types of incident fields, hard (i.e. Neumann) boundary conditions [5], [6] rather than soft (i.e. Dirichlet) boundary conditions, surfaces that are not perfectly-reflecting [1], and a coordinate system utilizing two spatial variables rather than one. Clearly, the work in this paper could be extended for application to a wider variety of physical situations, and the code developed here could serve as the foundation for numerical schemes to handle such generalizations.

REFERENCES

1. DeSanto, J.A., "Exact spectral formalism for rough-surface scattering," *J. Opt. Soc. Am. A*, **2**, 2202-2206 (1985).
2. Ref. 1, p. 2203.
3. Mathews, J., and R.L. Walker (1970), *Mathematical Methods of Physics*, Benjamin/Cummings, Menlo Park, California, 102.
4. Ref. 1, pp. 2204, 2205.
5. DeSanto, J.A., "Scattering from a sinusoid: derivation of linear equations for the field amplitudes," *J. Acoust. Soc. Am.*, **57**, 1196 (1975).
6. DeSanto, J.A., "Scattering from a perfectly reflecting arbitrary periodic surface: An exact theory," *Radio Sci.*, **16**, 1317-1318 (1981).
7. Omar, M.A. (1975), *Elementary Solid State Physics: Principles and Applications*, Addison-Wesley, Reading, Massachusetts, 35-37.
8. Bishop, G.C., and J. Smith, "A scattering model for nondifferentiable periodic surface roughness," *J. Acoust. Soc. Am.*, **91**, 744-770 (1992).
9. Chesneaux, J-M, and A. Wirgin, "Reflection from a corrugated surface revisited," *J. Acoust. Soc. Am.*, **96**, 1116-1129 (1994).
10. Jordan, A.K., and R.H. Lang, "Electromagnetic scattering patterns from sinusoidal surfaces," *Radio Sci.*, **14**, 1077-1088 (1979).
11. McCammon, D.F., and S.T. McDaniel, "Surface reflection: On the convergence of a series solution to a modified Helmholtz integral equation and the validity of the Kirchhoff approximation," *J. Acoust. Soc. Am.*, **79**, 64-70 (1986).

12. McCammon, D.F., and S.T. McDaniel, "Application of a new theoretical treatment to an old problem; sinusoidal pressure release boundary scattering," *J. Acoust. Soc. Am.*, **78**, 149-156 (1985).
13. Ref. 6, p. 1317.
14. Ref. 10, p. 1077.
15. Porter, D., and D.S.G. Stirling (1990), *Integral Equations, a Practical Treatment from Spectral Theory to Applications*, Cambridge, New York, 2-7.
16. Burden, R.L., and J.D. Faires (1993), *Numerical Analysis*, PWS, Boston, 174-182.
17. Ref. 16, pp. 98-108.
18. Noble, B., and J.W. Daniel (1988), *Applied Linear Algebra*, Prentice-Hall, Englewood Cliffs, New Jersey, 317-318.
19. Ref. 18, pp. 388-394.
20. Ref. 18, pp. 338-345.
21. Ref. 18, pp. 236-241.
22. Ref. 18, pp. 346-350.
23. Golub, G.H., and C.F. Van Loan (1989), *Matrix Computations*, Johns Hopkins, Baltimore, 561-569.
24. Ref. 16, pp. 192-198.
25. Golub, G.H., and J.M. Ortega (1992), *Scientific Computing and Differential Equations, An Introduction to Numerical Methods*, Academic Press, San Diego, 116-117.
26. Ref. 23, p. 570.
27. Ref. 23, pp. 562-564.

APPENDIX A - DRIVER CODE

```

implicit none
c
integer i,j,k,n
parameter (n=83)
integer lda,ldu,ldv,ldx
integer job,info,ipvt(n),rank,phys
integer inabv,inbel,outbel,nin,nout,t(n)
double precision pi,k1,L,d,nu(n),eta(n),xm(n),sx(n)
double precision rkern(n,n),ikern(n,n)
double precision alfa,beta
double precision rcond,eng,resnorm,diff,scang,angle
double precision coefA(n),coefB(n),coefC(n)
complex*16 a(n,n),x(n,n),f(n),N1(n),amp(n),res(n),aplust(n,n)
complex*16 s(n),e(n),u(n,n),v(n,n),work(n),z(n)
c
lda=n
ldu=n
ldv=n
ldx=n
pi=4.*datan(1.0d0)
k1=2.*pi
c
open(unit=1,file='output')
c
70  format('Length (wavelengths) :',16x,f8.4)
71  format('d/L',36x,f6.3)
72  format('Incident Angle (degrees) :',13x,f4.1)
73  format('Total Number of Samples :',13x,i3)
74  format('Samples per Wavelength :',15x,f5.2)
75  format('# of Physical Scattered Angles :',6x,i3)
76  format('Position of Surface :',17x,'Low')
77  format('Effective Rank Used :',17x,i3)
78  format(2x,'Bragg',8x,'Scattered',22x,'Scattered Amplitudes')
79  format(2x,'Index',10x,'Angle',15x,'Magnitude',8x,'real',8x,
x  'imaginary')
80  format(2x,i4,11x,f5.1,12x,f11.6,4x,f11.6,3x,f11.6)

```

```
      81  format('Energy :',30x,f18.14)
      82  format('Condition Number :',22x,e10.4)
c
c
c Surface characteristics:
c
L=20.0005
d=1.0
c
c
c Characteristics of incident field:
c
angle=0.0
if (abs(angle).ge.90.) then
  write(1,*) "The angle of incidence must be within
    x 90 degrees of normal incidence"
  write(6,*) "The angle of incidence must be within
    x 90 degrees of normal incidence"
  goto 99
endif
alfa=dsin(angle*pi/180.)
beta=dsqrt(1.-alfa*alfa)
c
write(1,70) L
write(1,71) d/L
write(1,72) angle
write(1,73) n
write(1,74) n/L
c
c
c Set grid for nu, determine corresponding eta:
c
i=0
  10  i=i-1
if ((alfa+i/L).gt.-1.) goto 10
inbel=-(i+1)
i=0
  12  i=i+1
if ((alfa+i/L).lt.1.) goto 12
inabv=i-1
```

```

nin=inbel+inabv+1
if (n.lt.nin) then
  write(1,*) "There are not enough samples to include
    x all scattered waves"
  write(6,*) "There are not enough samples to include
    x all scattered waves"
  goto 99
endif
nout=n-nin
outbel=(nout-mod(nout,2))/2
do 14 i=1,n
t(i)=i-(outbel+inbel+1)
nu(i)=alfa+t(i)/L
if (abs(nu(i)).le.1.) then
  eta(i)=dsqrt(1.-nu(i)*nu(i))
else
  eta(i)=dsqrt(nu(i)*nu(i)-1.)
endif
  14 continue
c
c
c Set grid for x, determine corresponding s(x):
c
do 16 j=1,n
if (j.lt.(n/2.)) then
  xm(j)=(2.*j-n)*L/(2.*(n-1.))
else
  xm(j)=(2.*j-1.-n)*L/(2.*(n-1.))
endif
  16 sx(j)=-((d/2.)*(1.+cos(2.*pi*xm(j)/L)))
c
c
c Determine the entries of the matrix of discretized kernels:
c
do 18 i=1,n
do 20 j=1,n
if (abs(nu(i)).le.1.) then
  rkern(i,j)=cos(k1*(eta(i)*sx(j)-nu(i)*xm(j)))
  ikern(i,j)=sin(k1*(eta(i)*sx(j)-nu(i)*xm(j)))
else

```

```

    rkern(i,j)=exp(-k1*eta(i)*sx(j))*cos(k1*nu(i)*xm(j))
    ikern(i,j)=-exp(-k1*eta(i)*sx(j))*sin(k1*nu(i)*xm(j))
endif
    20  x(i,j)=dcmplx(rkern(i,j),ikern(i,j))
    18  continue
do 22 j=2,(n-1),2
coefA(j)=2.*(xm(j)-xm(j-1))-(xm(j+1)-xm(j))
coefA(j)=coefA(j)*(xm(j+1)-xm(j-1))/(6.*(xm(j)-xm(j-1)))
coefB(j)=(xm(j+1)-xm(j-1))*3.
coefB(j)=coefB(j)/(6.*(xm(j)-xm(j-1))*(xm(j+1)-xm(j)))
coefC(j)=2.*(xm(j+1)-xm(j))-(xm(j)-xm(j-1))
    22  coefC(j)=coefC(j)*(xm(j+1)-xm(j-1))/(6.*(xm(j+1)-xm(j)))
do 24 i=1,n
x(i,1)=coefA(2)*x(i,1)
a(i,1)=x(i,1)
x(i,n)=coefC(n-1)*x(i,n)
a(i,n)=x(i,n)
do 26 j=2,(n-1),2
x(i,j)=coefB(j)*x(i,j)
    26  a(i,j)=x(i,j)
do 28 j=3,(n-2),2
x(i,j)=(coefA(j+1)+coefC(j-1))*x(i,j)
    28  a(i,j)=x(i,j)
    24  continue
c
c
c
c Determine RH side vector:
c
do 30 i=1,n
if (t(i).eq.0) then
    f(i)=-2.*beta*L
else
    f(i)=0.
endif
    30  continue
c
c
c Determine SVD of K:
c

```

```
job=11
call zsvdc(x,ldx,n,n,s,e,u,ldu,v,ldv,work,job,info)
c
c
c Determine the pseudo-inverse of K:
c
rank=n+1
  32  rank=rank-1
if (zabs(s(rank)).lt.(1.e-16)) goto 32
c
do 34 i=1,n
do 36 j=1,n
aplus(i,j)=dcmplx(0.,0.)
do 38 k=1,rank
  38  aplus(i,j)=aplus(i,j)+v(i,k)*dconjg(u(j,k))/s(k)
  36  continue
  34  continue
c
c
c Find N1 = K+ * f :
c
do 40 i=1,n
N1(i)=dcmplx(0.,0.)
do 42 j=1,n
  42  N1(i)=N1(i)+aplus(i,j)*f(j)
  40  continue
c
c Determine Residual:
c
do 44 i=1,n
res(i)=dcmplx(0.,0.)
do 46 j=1,n
  46  res(i)=res(i)+a(i,j)*N1(j)
  44  continue
resnorm=0.
do 48 i=1,n
res(i)=f(i)-res(i)
  48  resnorm=resnorm+zabs(res(i))*zabs(res(i))
resnorm=dsqrt(resnorm)
c
```

```

c Solve for the scattered amplitudes:
c
phys=0
do 50 i=1,n
if (abs(nu(i)).ge.1.) goto 50
phys=phys+1
do 52 j=1,n
rkern(i,j)=cos(k1*(eta(i)*sx(j)+nu(i)*xm(j)))
    ikern(i,j)=-sin(k1*(eta(i)*sx(j)+nu(i)*xm(j)))
    52  x(i,j)=dcmplx(rkern(i,j),ikern(i,j))
    50  continue
write(1,75) phys
write(1,76)
write(1,77) rank
write(1,*)
write(1,*)
write(1,78)
write(1,79)
write(1,*)
do 54 i=1,n
if (abs(nu(i)).ge.1.) goto 54
amp(i)=coefA(2)*x(i,1)*N1(1)+coefC(n-1)*x(i,n)*N1(n)
do 56 j=2,(n-1),2
    56  amp(i)=amp(i)+coefB(j)*x(i,j)*N1(j)
do 58 j=3,(n-2),2
    58  amp(i)=amp(i)+(coefA(j+1)+coefC(j-1))*x(i,j)*N1(j)
amp(i)=amp(i)/(2.*eta(i)*L)
scang=asin(nu(i))*180./pi
write(1,80) t(i),scang,zabs(amp(i)),
    x dreal(amp(i)),dimag(amp(i))
    54  continue
write(1,*)
write(1,*)
c
c
c Energy conservation check:
c
eng=0.
do 60 i=1,n
if (abs(nu(i)).ge.1.) goto 60

```

```
eng=eng+(eta(i)/beta)*zabs(amp(i))*zabs(amp(i))
  60  continue
c
c
c Obtain condition number of original X and its inverse:
c
call zgeco(a,lda,n,ipvt,rcond,z)
if (info.ne.0) write(6,*) "Warning:  info =",info
c
write(1,81) eng
write(1,82) 1./rcond
c
  99  continue
c
end
```